Extrachromosomal DNA micronucleation constrains tumour fitness and improves patient survival

Lotte Brückner[1,2,3*], Robin Xu[2,3*], Jun Tang[4,5*], Aditi Gnanasekar[4,5], Alexander Herrmann[2], Ivy Tsz-Lo Wong[4,5], Shu Zhang[4,5], Fengyu Tu[6], Madison Pilon[2], Alexander Kukalev[1,7], Katharina Pardon[2,3], Olga Sidorova[2,3], Joshua Atta[2,3], Qinghao Yu[2,3], Giulia Montouri[2,3], Davide Pradella[8], Mila Ilić[9], Kentaro Suina[10], Marco Novais-Cruz[9], Sarah Kaltenbach[11], Denise Treue[12], Mădălina Giurgiu-Kraljič[2,3], Sergej Herzog[1,7], Ann-Sophie Hollinger[2,3], Nadine Wittstruck[2,3], Martina Fernandez[2,3], Nicole Wolozyn[2], Finnja Becker[2,3], Varvara-Rigina Louma[2,3], Xiaowei Yan[4,5], Rachel Schmargon[2,3], Jan Dörr[2,3], David Gamlin[2,3], Annika Lehmann[12], , Dennis Gürgen[13], Matthias Richter[14], Frank Dubois[12], Fabrizio Simeoni[15], Betheney R. Pennycook[15], Alastair Hamilton[15], Ralph K. Lindemann[15], Courtney Dawes[16], Gabriel Balmus[17,18,19] Barbara Hero[20], Matthias Fischer[20,21], Vineet Bafna[22], Roel Verhaak[10,23], Geoffrey Wahl[24], Yang Liu[16], Richard P. Koche[25], Stamatis Papathanasiou[11], René Medema[9], Bastiaan Spanjaard[2,3], Andrea Ventura[8], Ana Pombo[1,7,26,27], Weini Huang[28], Monika Scheer[2], Benjamin Werner[29], Howard Y. Chang[30#], Paul S. Mischel[4,5#], Anton G. Henssen[1,2,3,31c#]

[1]Max Delbrück Center for Molecular Medicine, Berlin, Germany
[2]Department of Pediatric Oncology/Hematology, Charité-Universitätsmedizin Berlin, Germany
[3]Experimental and Clinical Research Center (ECRC) of the MDC and Charité Berlin, Berlin, Germany
[4] Department of Pathology, Stanford University School of Medicine
[5] Sarafan ChEM-H, Stanford University
[6] Group of Theoretical Biology, The State Key Laboratory of Bio-control, School of Life Sciences, Sun Yat-sen University, Guangzhou 510275, People's Republic of China
[7]Max-Delbrück Centre for Molecular Medicine, Berlin Institute for Medical Systems Biology, Epigenetic Regulation and Chromatin Architecture Group, Berlin, Germany
[8]Cancer Biology and Genetics Program, Memorial Sloan Kettering Cancer Center, New York, NY, USA
[9]Oncode Institute and Princess Máxima Center for Pediatric Oncology, Utrecht, The Netherlands
[10]Department of Neurosurgery, School of Medicine, Yale University, New Haven, USA.
[11]Institute of Molecular Biology, Mainz, Germany
[12]Institute of pathology, Charité-Universitätsmedizin Berlin, corporate member of Freie Universität Berlin, Humboldt-Universität zu Berlin, Berlin, Germany
[13]Experimental Pharmacology and Oncology (EPO), Berlin, Germany
[14]Advanced Light Microscopy, Max Delbrück Center for Molecular Medicine in the Helmholtz Association, Robert-Rössle-Straße 10, 13125, Berlin, Germany
[15]Econic Biosciences, London, United Kingdom
[16] Department of Biochemistry, University of Utah, Salt Lake City, UT, USA
[17]UK Dementia Research Institute, University of Cambridge, Cambridge, UK

[18]Department of Clinical Neurosciences and NIHR Biomedical Research Centre, University of Cambridge, Cambridge, UK
[19]Department of Molecular Neuroscience, Transylvanian Institute of Neuroscience, Cluj-Napoca, Romania
[20]Department of Experimental Pediatric Oncology, University Children's Hospital of Cologne, Medical Faculty, Cologne, Germany
[21]Center for Molecular Medicine Cologne (CMMC), Medical Faculty, University of Cologne, Cologne, Germany
[22]University of San Diego, California, USA
[23]Department of Neurosurgery, Amsterdam University Medical Centers/VUmc, Amsterdam, the Netherlands
[24]Salk Institute for Biological Studies, San Diego, USA
[25]Center for Epigenetics Research, Memorial Sloan Kettering Cancer Center, New York, NY, USA
[26]Institute of Biology, Humboldt-Universität zu Berlin, Berlin, Germany
[27]Berlin Institute of Health, Berlin, Germany
[28]Queen Mary University of London, London, UK
[29]Evolutionary Dynamics Group, Centre for Cancer Evolution, Barts Cancer Institute, Queen Mary [30]Departments of Dermatology, Genetics, and Pathology, Stanford University School of Medicine
University London, UK
[31]German Cancer Consortium (DKTK), partner site Berlin, and German Cancer Research Center (DKFZ), Heidelberg, Germany
*These authors contributed equally to this work.
[#] These authors co-supervised this work.
Correspondence should be addressed to Anton G. Henssen (henssenlab@gmail.com, +49(0)30450666118) and Paul S. Mischel (pmischel@stanford.edu).

Conflict of interest

A.G.H and R.P.K are founders of Econic Biosciences. F.S., B.P., A.H., and R.L. are employees of Econic Bioscience. P.S.M. is a co-founder of Boundless Bio. He has equity and chairs the scientific advisory board, for which he is compensated. H.Y.C. is a co-founder of Accent Therapeutics, Boundless Bio, Cartography Biosciences, and Orbital Therapeutics and was an advisor to 10x Genomics, Arsenal Biosciences, Chroma Medicine, and Exai Bio until Dec 15, 2024. H.Y.C. is an employee and stockholder of Amgen as of Dec. 16, 2024. G.B. is the founder and chief executive officer (part time) of Function RX Ltd. The other authors declare no potential conflicts of interest.

Abstract

Extrachromosomal DNA (ecDNA) contributes to cancer genome instability by enabling high-copy oncogene amplification, intratumoural heterogeneity and rapid genetic change. Micronuclei (MN) are frequently observed in chromosomally unstable cancers, yet their origins and relevance in ecDNA-driven tumours remain incompletely understood. Here, we investigate the relationship between ecDNA segregation errors and MN formation. We find that ecDNA frequently localizes to MN and represents a prominent source of MN content in ecDNA-positive cancer cells. Mitotic clustering of oncogene-bearing ecDNAs is associated with asymmetric inheritance and mis-segregation into MN. Transfer of oncogenes from ecDNA into MN is accompanied by reduced transcriptional output. Single-MN sequencing shows that individual MN are enriched for ecDNA to a degree that exceeds expectations from stochastic mis-segregation and that in MN oncogenes originating from multiple distinct ecDNAs coalesce. Using live-cell imaging, we observe that cells inheriting ecDNA-positive MN show limited proliferative capacity and an increased likelihood of cell death. In neuroblastoma patients with *MYCN*-amplified ecDNA, higher frequencies of ecDNA-positive MN at diagnosis are associated with improved event-free and overall survival. Together, these findings link ecDNA mis-segregation to MN formation and reduced cellular fitness, suggesting that ecDNA-positive MN may reflect a state of impaired oncogenic ecDNA function with potential relevance for clinical outcome.

Introduction

Extrachromosomal DNA (ecDNA) has emerged as a major form of cancer genome instability, driving high-copy oncogene amplification, intratumoural heterogeneity, rapid tumour evolution, and therapy resistance[1,2]. Across diverse cancer types, the presence of ecDNA (ecDNA$^+$) correlates with poor outcomes compared to tumours with linear chromosomal amplifications or other types of genome instability[3]. EcDNAs are relatively large (approximately 1-2Mb)[4], chromatinized, circular DNA structures that are enriched for oncogenes, as well as regulatory and immunomodulatory elements[5-7]. They are observed specifically in cancer cells and are distinct from extrachromosomal circular DNA (eccDNA), which comprise smaller, typically non-clonal circular DNA elements that rarely encompass full genes and can also be detected in normal cells[8-10]. Their absence of centromeres on ecDNA[11,12], permits uneven segregation during mitosis, fuelling heterogeneity and accelerating tumour evolution through non-Mendelian inheritance[11]. Chromosomal tethering mechanisms are thought to promote ecDNA transmission during cell division[13,14].

Micronuclei (MN) are small, extranuclear bodies initially enclosed by nuclear envelopes containing mis-segregated chromosomes or chromatin fragments arising during mitosis[15,16], distinguishing them from other extranuclear structures such as exclusomes[17]. They are a hallmark of chromosomal instability. Chromatin in MN can undergo chromothripsis[18-20] and epigenetic remodelling[21-23], resulting in long-term genomic and transcriptional alterations. MN can serve as intermediates for ecDNA generation[20], suggesting reciprocal links between ecDNA and MN biology. Treatment of ecDNA-bearing cells with hydroxyurea or other DNA-damaging agents increases MN frequency and decreases oncogene levels, implying that damaged ecDNA may seed MN formation[24-26]. However, the mechanisms of MN generation in ecDNA$^+$ tumours, their molecular composition, and functional consequences remain unknown.

Using cell lines, engineered mouse models, patient tumour samples, single-MN sequencing, and live-cell imaging, we set out to define how micronucleation arises from ecDNA and how this process shapes cancer cell fitness and patient outcome.

Main

ecDNA gives rise to oncogene-containing micronuclei

To assess how frequently ecDNA is incorporated into micronuclei (MN) and how faithfully it is retained during cell division, we compared near-isogenic cancer cell lines carrying oncogene amplifications either on ecDNA or re-integrated as homogeneously staining

124 regions (HSRs). (Fig. 1a, Extended Fig. 1). Across three such pairs, COLO 320DM/HSR
125 (*MYC*), GBM39EC/HSR (*EGFR*vIII), and PC3-DM/HSR (*MYC*), ecDNA$^+$ cells displayed
126 significantly higher frequencies of oncogene-positive MN (oncogene$^+$ MN) than their HSR
127 counterparts (Fig. 1b). In contrast, the frequency of oncogene$^-$ MN was similar, indicating that
128 ecDNA mis-segregation contributes to elevated MN frequency (Fig. 1b-c). Lamin B1
129 expression was higher in oncogene$^+$ MN than oncogene$^-$ MN in ecDNA$^+$ cell lines, suggesting
130 that oncogene+ MN have an intact inner nuclear membrane (Extended Fig. 2a-c). Analysis of
131 275 patient tumour biopsies from diverse cancer types with FISH-defined amplification status
132 of distinct oncogenes (Fig. 1d, Supplementary table 1) confirmed this pattern: ecDNA$^+$ tumours
133 contained a significantly greater fraction of cells with MN than non-amplified tumours or
134 tumours with chromosomal amplifications, and the proportion of oncogene$^+$ MN was
135 correspondingly higher (Fig. 1e-f, Extended Fig. 2d). Micronuclei in ecDNA$^+$ cells were
136 smaller than those in HSR cells, consistent with their predominant composition of ecDNA
137 rather than larger chromosomal fragments (Extended Fig. 2e). MN abundance positively scaled
138 with overall ecDNA copy number in most tumour types (Fig. 1g–j, Extended Fig. 2f). A
139 binomial segregation model estimated an ecDNA mis-segregation rate of 1.7% (range 0–7.8%),
140 indicating overall efficient, but occasionally faulty, retention during mitosis (Extended Data
141 Fig. 2g).
142 To rule out high oncogene expression as the cause of increased MN formation, we
143 analysed *p53*$^{fl/fl}$*;Myc*$^{ec/+}$ mouse adult neural stem cells (aNSCs) transduced to express Cre
144 recombinase, which results in engineered *Myc*-containing ecDNAs, compared to
145 *p53fl/fl;Myc*^{OE} control cells with chromosomally integrated *Myc* that express comparably high
146 levels of Myc protein (Fig. 1k). Only ecDNA$^+$ cells exhibited elevated MN abundance, and
147 these MN were enriched for *Myc* sequences (Fig. 1l). Thus, the presence of ecDNA is linked
148 to elevated MN frequencies in cancer cells.
149
150 ***Replication stress and DNA damage promote ecDNA cluster detachment and micronucleus***
151 ***formation during mitosis***
152 Because ecDNAs lack centromeres, they can rely on chromosomal tethering to ensure
153 inheritance during mitosis[11,14,27]. We hypothesized that MN formation could occur when
154 ecDNAs fail to tether to chromosomes during cell division (Fig. 2a), as also evidenced by
155 recent reports[14,28]. If ecDNAs detached and mis-segregated stochastically and remained
156 independent, individual ecDNA molecules would be expected to segregate into separate
157 micronuclei and be inherited by both daughter cells. Instead, live-cell imaging of unperturbed

158 COLO 320DM cells expressing fluorescently labelled *MYC* ecDNA (tetR–mNeonGreen) and
159 chromatin (H2B–emiRFP670)[27] revealed that ecDNA detach from chromatids as clusters
160 during mitosis and are subsequently encapsulated on average into single MN in daughter cells
161 (Fig. 2a-b, Supplementary Video 1). The frequency of detached clusters positively scaled with
162 the abundance of ecDNA in cells (Fig. 2c–d), suggesting that while individual detachment
163 events may occur stochastically, ecDNA coalescence and subsequent mis-segregation are
164 governed by non-random processes.

165 ecDNAs are frequently damaged and prone to replication stress[29,30], prompting us to
166 test whether DNA damage promotes clustered detachment and micronucleation. Consistent
167 with these prior findings, significantly higher signs of replication stress and DNA damage were
168 observed on ecDNA compared to HSR (Extended Fig. 3a-f). Treatment with hydroxyurea,
169 which induces replication stress and causes DNA damage by depleting nucleotides, increased
170 signs of replication stress especially on ecDNA (Extended Fig. 3a-f). Nanopore-based fork
171 progression analysis confirmed reduced nucleotide incorporation and disproportional
172 replication fork slowing on ecDNA both in untreated conditions and upon HU (Extended Fig.
173 4). This resulted in substantially more untethered, γH2AX-positive ecDNA$^+$ clusters during
174 anaphase in COLO 320DM cells compared to their isogenic HSR counterparts as well as in
175 non-isogenic cell line pairs (Fig. 2e-g, Extended Fig. 5). As a result, ecDNA$^+$ cells exhibited
176 increased MN frequency, and MN were significantly enriched for ecDNA oncogene sequences
177 (oncogene$^+$ MN) to an extent exceeding expectations from random segregation (Extended Fig.
178 6a-b). The increase in MN abundance was rescued by transfection of nucleotides, confirming
179 that HU-induced nucleotide depletion promoted MN formation (Extended Fig. 6c-d). No
180 enrichment of MN for oncogene sequences was observed in cells with chromosomal
181 amplifications, in which the overall MN rate increased following hydroxyurea, but those MN
182 did not contain oncogene sequences (oncogene$^-$ MN, Fig. 2h–j, Extended Fig. 6e-f). The
183 frequency of MN after hydroxyurea scaled with the abundance of ecDNA in cells (Extended
184 Fig. 6g-h). As in untreated cells, despite cells harbouring high numbers of the same ecDNA
185 species, each daughter cell typically contained only a single MN (mean 1.03 and 1.19 per cell
186 for CHP212 and COLO 320DM, respectively), suggesting that detached ecDNAs coalesce into
187 a single cluster before segregation and micronucleation in one daughter cell. Targeted
188 CRISPR–Cas9 cleavage of ecDNA reproduced this effect, producing untethered ecDNA
189 clusters that segregated into MN (Fig. 2k–l, Extended Fig. 7), suggesting that damage on
190 ecDNA promotes clustered detachment and micronucleation. Thus, ecDNA is more prone than

191 chromosomal amplifications to respond to replication stress with clustered detachment in
192 mitosis, resulting in micronucleus formation.
193 The MDC1–CIP2A–TOPBP1 complex stabilizes damaged chromosomal fragments
194 during mitosis[31,32], raising the possibility that it mediates ecDNA clustering following their
195 damage. Immunofluorescence staining revealed that a subset of detached clusters colocalised
196 with CIP2A, and TOPBP1 (Fig. 2m), with overall signal intensity increasing after hydroxyurea
197 treatment (Fig. 2n, Extended Fig. 8a-b). Pharmacological reduction of CIP2A expression using
198 TD19 dispersed Hoechst-stained clusters into individual foci in ecDNA+ cells, and increased
199 the number of small MN per cell without changing the overall fraction of micronucleated cells
200 (Extended Data Fig. 8c-h). Similarly, shRNA-mediated knockdown of CIP2A, TOPBP1, or
201 MDC1 diminished chromatin clustering during anaphase, while not changing overall
202 detachment frequency (Fig. 2o-p, Extended Fig. 8i-j). Together, these results indicate that the
203 MDC1–CIP2A–TOPBP1 complex is at least in part required for the coalescence of damaged
204 ecDNAs into clusters, similar to what was described for pulverized DNA during
205 chromothripsis[31,32], which are then inherited as a single MN in daughter cells. This pathway
206 links replication stress to elevated ecDNA mis-segregation and micronucleus formation.
207
208 ***Single-micronucleus sequencing reveals that multiple distinct ecDNAs tend to coalesce into***
209 ***the same micronucleus***
210 Up to 25% of ecDNA$^+$ tumours harbour more than one ecDNA species[27]. Given
211 damaged ecDNAs cluster before the end of mitosis, individual micronuclei might contain
212 oncogenes from distinct ecDNA species. At the same time, DNA damage could in principle
213 generate chromosomal fragments that co-segregate into MN together with attached ecDNA.
214 To determine the genomic content of MN in cancer cell lines with multiple ecDNA species,
215 we developed a laser-microdissection method to isolate single MN and their corresponding
216 primary nuclei, followed by paired-end sequencing (Fig. 3a). This approach was applied to TR-
217 14 cells, which harbor multiple ecDNA species, each carrying a distinct oncogene (eg. *MYCN*,
218 *MDM2*, or *CDK4*) alongside additional passenger genes. The circular structure of these ecDNA
219 was previously assessed by sequence reconstruction[33], and their extrachromosomal presence,
220 oncogene content and copy number per cell was confirmed by metaphase-FISH (Fig. 3b). After
221 hydroxyurea treatment to induce replication stress, 70% of micronuclei were strongly enriched
222 in all ecDNA species (Fig. 3c; Extended Fig. 9a-b), consistent with collective micronucleation
223 of separate ecDNAs after replication stress. Notably, the majority of ecDNA$^+$ MN (92.3%)
224 lacked detectable linear chromatin fragments, arguing against frequent co-segregation of

225 chromosomal fragments together with ecDNA and indicating that ecDNA mis-segregates more
226 readily than chromosomal DNA under replication stress (Fig. 3d-e; Extended Fig. 9c).
227 Importantly, ecDNA was markedly enriched relative to linear chromosomal DNA in
228 micronuclei compared with the corresponding primary nuclei, a pattern that would not be
229 expected if ecDNA mis-segregated stochastically, in which case similar relative enrichments
230 would be anticipated in both compartments. Copy number proportions among ecDNA species
231 within individual MN mirrored those in the primary nucleus (Fig. 3f, Extended Fig. 9d), and
232 enrichment of different ecDNA species correlated positively in MN (Fig. 3g-j), in line with the
233 collective micronucleation of structurally distinct ecDNAs.
234 To test whether damage to one ecDNA species can result in collective micronucleation
235 of other ecDNA species, we introduced CRISPR–Cas9-mediated double-strand breaks on *MYC*
236 ecDNA of DMS273 cells, which also harbour a separate ecDNA species encoding for *MYCL*
237 (Extended Fig. 10a). Targeted cleavage increased γH2AX foci on *MYC* and promoted its
238 presence in MN, while concurrently enriching *MYCL* ecDNA in the same MN (Fig. 3k,
239 Extended Fig. 10b-f).
240 Taken together, these findings suggest that ecDNA mis-segregate into micronuclei *en*
241 *masse* in cells with elevated ecDNA damage and is largely independent of linear chromatin
242 fragments, raising the possibility that this impacts ecDNA inheritance patterns (Extended Fig.
243 11).
244
245 ***Micronucleation leads to asymmetric inheritance of ecDNA with reduced oncogenic***
246 ***transcription***
247 Live-cell imaging revealed that ecDNA clusters, both under basal conditions and
248 following hydroxyurea treatment, segregated on average into a single micronucleus (MN) and
249 one of the two daughter cells, suggesting that micronucleation introduces asymmetry into
250 ecDNA inheritance (Extended Fig. 12a-b, Supplementary Video 2-3). This suggests that
251 ecDNA micronucleation skews previously observed random inheritance patterns[11], which
252 would have implications for tumour evolution. To quantify this effect, we measured ecDNA
253 copy number in paired daughter cells at cytokinesis using DNA FISH after hydroxyurea
254 treatment. Compared to untreated controls, hydroxyurea markedly increased the degree of
255 ecDNA imbalance between daughter cells (Extended Fig. 12b), confirming that replication
256 stress promotes asymmetric segregation through micronucleation.
257 To further investigate the consequence of asymmetric segregation for the inheritance
258 of ecDNA, we developed a computational model (Extended Fig. 12c). Assuming a probability

259 q of asymmetric segregation and probability 1-q of random segregation. The resulting ecDNA
260 distribution in daughter cells shifted from unimodal (random segregation) to bimodal or
261 trimodal patterns as q and p_1 varied (Extended Data Fig. 12d). Using an approximate Bayesian
262 computation framework (ABC), we inferred optimal parameter estimates for p_1 and q
263 (Extended Data Fig. 11e-i). Applying this to our experimental data from pairs of daughter cells
264 with and without hydroxyurea treatment, we observed increased biased segregation post-
265 treatment (Extended Fig. 12j-l). Thus, replication stress enhances ecDNA segregation
266 asymmetry (Fig. 11).
267 Linear chromatin fragments incorporated in MN remain epigenetically and
268 transcriptionally silenced[21-23]. We set out to test if ecDNA is also repressed in MN following
269 replication stress (Extended Fig. 13a). During mitosis, ecDNA retained high H3K27Ac and
270 low H3K27me3, much unlike chromosomal DNA, which showed the expected inactive
271 chromatin patterns (Extended Fig. 13b-c). However, ecDNA in MN had significantly reduced
272 H3K27Ac and stably low H3K27me3 compared to ecDNA in mitosis and the primary nuclei
273 following hydroxyurea treatment (Extended Fig. 13d-e). Chromatin immunoprecipitation
274 sequencing confirmed reduced H3K27ac at ecDNA loci, including *MYC* (Extended Fig. 13f).
275 Micronuclei also exhibited significantly lower levels of pRNAPII-S5, indicating reduced
276 transcriptional activity in micronuclei (Extended Fig. 13g-h). Indeed, intron RNA-FISH further
277 confirmed that most micronuclei in ecDNA-containing cell lines lacked detectable oncogene
278 expression, independent of the oncogene encoded (Extended Fig. 13i). RNA sequencing
279 confirmed the decreased expression of ecDNA-encoded genes, including *MYC*, alongside
280 reduced MYC-driven transcriptional programs (Extended Fig. 13j-l). Collectively, these results
281 show that, unlike its high expression in the nucleus and throughout mitosis[27,28], ecDNA within
282 micronuclei is transcriptionally silenced, suggesting that micronucleation restrains the
283 oncogenic potential of ecDNA.
284
285 ***ecDNA micronucleation impacts cancer cell fitness and is associated with improved patient***
286 ***survival***
287 To investigate the functional consequences of ecDNA$^+$ micronuclei, we performed live-
288 cell imaging under both untreated conditions and following hydroxyurea exposure to track
289 daughter cells inheriting a micronucleus after mitosis (Fig. 4a). Cells that inherited large,
290 ecDNA-containing MN (> 2 μm diameter) showed delayed progression to the next division,
291 and higher death rates than the daughter cell lacking a MN (Fig. 4b–c; Extended Fig. 14a-b,
292 Supplementary video 4-6). These effects were independent of ecDNA copy number in the

293 primary nucleus (Extended Fig. 14c-d), but were strongest when MN contained high ecDNA
294 content, indicating that ecDNA in MN impose a direct fitness penalty.
295 If this penalty constrains tumour growth, patients whose tumours contain abundant
296 ecDNA$^+$ MN should have less aggressive disease. We examined diagnostic biopsies from 387
297 patients and selected 86 children with *MYCN*-amplified neuroblastoma in which ecDNA was
298 identified by FISH before treatment (Fig. 4d, Extended Fig. 15a). For each case, we quantified
299 the proportion and ecDNA content of MN at baseline and compared these with clinical outcome
300 after standard-of-care treatment. Neither total ecDNA copy number in the primary nucleus nor
301 overall MN frequency correlated with survival (Extended Fig. 15b-g). In contrast, tumours with
302 a high fraction of ecDNA$^+$ MN exhibited significantly longer event-free and overall survival
303 than tumours with few or no ecDNA$^+$ MN (Fig. 4e; Extended Data Fig. 15h). Modelled as a
304 continuous variable and assuming linearity, ecDNA$^+$ MN frequency remained independently
305 prognostic (Overall survival: hazard ratio 0.951, 95% CI 0.914–0.990, p = 0.015, event-free
306 survival: hazard ratio 0.956, 95% CI 0.923–0.990, p = 0.012), corresponding to a 4.9 %
307 reduction in risk of death for every 1 % increase in ecDNA$^+$ MN. These findings indicate that
308 an increase in micronuclei containing ecDNA (ecDNA$^+$ MN) is associated with impaired
309 proliferative capacity of cancer cells and reduced tumour fitness (Fig. 4f).
310 Our results support the view that faithful inheritance of ecDNA depends on
311 chromosomal tethering during mitosis[13,14,34]. When this process fails, oncogene-bearing
312 ecDNAs can coalesce into MDC1–CIP2A–TOPBP1–stabilized clusters that segregate
313 asymmetrically and are sequestered into micronuclei, a process that is potentiated by
314 replication stress–induced damage. This asymmetric accumulation of ecDNA within
315 micronuclei is associated with decreased oncogene output, impaired daughter-cell fitness and
316 corresponds to improved survival in children with *MYCN*-amplified neuroblastoma.
317 Together, these findings link ecDNA$^+$ micronucleus formation to reduced tumour
318 fitness, including at the patient level. The observation that sequestration of oncogene-
319 containing ecDNA into micronuclei is associated with a proliferative penalty and improved
320 event-free and overall survival in children with neuroblastoma highlights the functional
321 relevance of ecDNA-containing micronuclei and suggests their potential utility as biomarkers
322 for patient stratification and for therapeutic strategies aimed at selectively damaging ecDNA.
323
324
325

326 **Methods**

327 ***Cell lines***

328 Human tumour cell lines were obtained from the American Type Culture Collection (ATCC)
329 or a gift from collaborative laboratories. The identity of all cell lines was verified by short
330 tandem repeat genotyping (Eurofins Genomics). The absence of *Mycoplasma* sp.
331 contamination was determined using a Lonza MycoAlert system (Lonza). For this study, 11
332 ecDNA amplified cell lines (DMS273, STA-NB10DM, COLO320 DM, TR-14, CHP-212,
333 Lan5, UKF-NB6, KP-N-YN, PC3-DM, SiMA, SMS-KAN), 5 HSR amplified cell lines (STA-
334 NB10HSR, COLO 320HSR, PC3-HSR, NGP, IMR5/75), 2 non-amplified cancer cell line
335 (ShEP, HeLa) and 1 non-cancerous cell line (RPE-hTERT) were used. HEK293T cells were
336 used for virus production. Near isogenic cell line pairs GBM39ec, GBM39HSR, COLO320
337 DM, COLO320 HSR, PC3-DM, PC3-HSR cells were extensively characterized before[29].

338

339 ***Cell culture***

340 Most neuroblastoma and colon cancer cell lines were cultured in RPMI-1640 medium (Gibco)
341 supplemented with 1 % of penicillin, streptomycin, and 10 % of fetal calf serum (FCS) (Thermo
342 Fisher). STA-NB10DM and HSR cells were cultured in RPMI-1640 medium (Gibco)
343 supplemented with 1 % of penicillin, streptomycin, 10 % of fetal calf serum (FCS) (Thermo
344 Fisher), 1 % Glutamax (Thermo Fisher), 1 % Sodium Pyruvat (Thermo Fisher) and 10 mM
345 HEPES (Sigma). UKF-NB6 was cultured in IMDM medium (Gibco) supplemented with 1 %
346 of penicillin, streptomycin, and 10 % of FCS. RPE and HEK293T cells were cultured in
347 DMEM (Gibco) supplemented with 1 % of penicillin, streptomycin, and 10 % of FCS.
348 GBM39ec and GBM39HSR cell lines were cultured in Dulbecco's Modified Eagle's
349 Medium/F12 (Gibco, catalogue no. 11320-033) supplemented with 1× B27 (Gibco, catalogue
350 no. 17504-01), 20 ng/ml epidermal growth factor (Sigma, catalogue no. E9644), 20 ng/ml
351 fibroblast growth factor (Peprotech, catalogue no. AF-100-18B), 5 µg/ml heparin (Sigma,
352 catalogue no. H3149) and 1× GlutaMAX (Gibco, catalogue no. 35050-061). COLO 320DM,
353 COLO 320HSR, PC3-DM, PC3-HSR and COLO 320DM-Tg19 (live-cell imaging line) cells
354 were cultured in DMEM (Corning, #10-013-CV) with 1% PSQ and 10% FBS. To assess the
355 number of viable cells, cells were trypsinized (Thermo Fisher), resuspended in medium, and
356 sedimented at 300 *g* for 5 minutes. STA-NB10 cells were split using Accutase (Thermo
357 Fisher). HeLa cells were cultured in Advanced DMEM-F12 (Gibco) with addition of 10% FCS,
358 1% Penicillin-Streptomycin (Gibco) and 1% GlutaMax (Gibco). Cells were then resuspended
359 in medium, mixed in a 1:1 ratio with 0.02 % trypan blue (Thermo Fisher), and counted with a

360 Bio-Rad TC20 cell counter. CHP212-PIP-FUCCI (Nanopore-based replication fork dynamics)
361 cells were generated by lentiviral transduction of pLenti-PGK-Hygro-PIP-FUCCI (Addgene #
362 138714). Transduced cells were selected by FACS sorting 10 days after transduction and kept
363 under 100 µg/mL Hygromycin B selection.
364 In drug experiments, cells were treated for 24 or 72h with 50µM or 80 µM or 100µM
365 hydroxyurea or a combination of 80 µM hydroxyurea together with 1 µM TD-19 (Merck
366 Millipore, 532912) as indicated in figure legends respectively. Control cells were treated with
367 an equivalent volume of DMSO or H2O. Drug concentrations were selected based on cell
368 viability as assessed using the CellTiter-Glo Assay (Promega G7571). GBM39ec/GBM39HSR
369 cells were treated with 100 µM hydroxyurea for 5 and 72 hrs, EdU (10 µM) was added for 30
370 mins before fixing. dNTP supplementations were conducted at the indicated concentrations at
371 a 1:1 ratio with Lipofectamine 3000 (ThermoFisher, L3000001) according to manufactures
372 protocol.
373
374 ***Genetically induced ecDNA cell lines***
375 Adult Neuronal Stem Cells (aNSCs) were isolated from Mycec/+; p53fl/fl and p53fl/fl animals
376 described in Pradella et al.[35] and cultured following the protocol described by Ahmed et al.[36]
377 aNSC were maintained in laminin-coated (Sigma-Aldrich, L2020) dishes in NeuroCult Stem
378 Cell Basal Media with NeuroCult Proliferation Supplement (Mouse & Rat) (Stem Cells
379 Technologies, 05702), 20 ng ml−1 EGF (Stem Cells Technologies, 78006), 10 ng ml−1 bFGF
380 (Stem Cells Technologies, 78003), and 2 µg ml−1 heparin (Stem Cell Technologies, 07980).
381 Cells were tested for mycoplasma contamination and maintained in a humidified, 5% CO2
382 atmosphere at 37 °C. aNSC overexpressing Myc transgene were generated by infecting p53fl/fl
383 aNSC with pBABE-Puro-Myc retrovirus. Mycec/+; p53fl/fl and p53fl/fl aNSC were also
384 infected with pBABE-Puro retrovirus. Upon infection, cells were selected with puromycin
385 (1 µg ml−1; Sigma-Aldrich, P9620) for 3-4 days. Selected cells were then infected with AdCre
386 (ViraQuest, VQ-Ad-CMV-Cre; 1 × 1012particles per milliliter; 091317) to promote p53 loss
387 and Myc-containing ecDNA accumulation as described in Pradella et al.[35]
388
389 ***Retrovirus production***
390 pBABE-Puro-C-Myc plasmid was generated by site-directed mutagenesis from pBABE-Puro-
391 C-Myc T58A (Addgene #53178) by removing the T to A mutation in the mouse coding region.
392 For retrovirus production, HEK-293T cells were seeded in high-glucose Dulbecco's modified
393 Eagle medium (DMEM, 4.5 g l−1; Thermo Fisher Scientific, 11995065) supplemented with

394 10% heat-inactivated fetal bovine serum (FBS, Sigma-Aldrich, F2442) without antibiotics in
395 100 mm petri dishes. The next day, cells at approximately 60–70% confluence were transfected
396 with 20 µg of retroviral vector carrying the mouse C-Myc cDNA or a control vector, 5 µg of
397 packaging plasmid and 1 µg of envelope plasmid. After 24 h, the medium was replaced with
398 DMEM with antibiotics. Cells were incubated for 48 h with two consecutive collections of the
399 medium containing the retroviral particles at 24 and 48 h. Medium collected was filtered using
400 a 0.45 µm filter unit and used to transduce aNSC cells by incubating cells with viral supernatant
401 supplemented with polybrene (0.2 µl ml−1; Sigma, TR-1003G).
402
403 ***Antibodies for immunoblots***
404 For immunoblots of aNSCs the following primary antibodies were used: anti-vinculin (1:5000;
405 Millipore, MAB3574), anti-c-MYC (1:000; Cell Signaling, D84C12). The following secondary
406 antibodies were used: IRDye 800 anti-rabbit (LICOR, 926-32213) and IRDye 680 anti-mouse
407 (LICOR, 926-68072). For shRNA knockdown conformation, the following antibodies were
408 used: Anti-CIP2A (1:5000, Santa Cruz, sc-80659) , anti-TOPBP1 (1:5000, Sigma-Aldrich,
409 ABE1463), anti-MDC1(1:5000, abcam, ab11169), anti-vinculin (1:5000, Cell signalling,
410 4650S), goat anti-Mouse IgG (H+L) Cross-Adsorbed Secondary Antibody, Alexa Fluor™ 647
411 (1:5000, Invitrogen, A21235) and goat anti-rabbit IgG (H+L), horseradish peroxidase
412 conjugates (1:5000, Invitrogen, G21234) were used.
413
414 ***Antibodies or immunofluorescent staining:***
415 For staining for single-micronucleus sequencing, samples were incubated in mouse anti-pan-
416 histone H11-4 (1:500; Merck, MAB3422), followed by incubation with Alexa555 (1:1000;
417 Invitrogen, A-31570) or Alexa488 anti-mouse secondary antibody (1:1000; Invitrogen, A-
418 11001). For immunofluorescent staining followed by imaging, the following primary
419 antibodies were used: anti- pRPA2-S33 (1:1000, Novus Biological, NB100-544), anti-Lamin
420 B1 Monoclonal antibody (proteintech, 66095-1-Ig, IF - 1:500), Anti-H2AX (1:500/ 1:250,
421 Sigma Aldrich, 05-636), anti-CIP2A (1:500, Santa Cruz, sc-80659), anti-TOPBP1 (1:500,
422 Sigma-Aldrich, ABE1463), anti-pRNAPolII(Serine5, 1:500, Merck, MABE954), anti-
423 H3K27ac (1:500, Active Motif, 39133) or anti-H3K27me3 (1:500, Thermo Fisher, G.299.10).
424 Followed by incubation with secondary antibodies: Alexa Fluor 647, Goat anti-Rabbit IgG
425 (H+L) Cross-Adsorbed Secondary Antibody (1:1000, Invitrogen, A21244) and goat anti-
426 Mouse IgG (H+L) Cross-Adsorbed Secondary Antibody, Alexa Fluor™ 647 (1:1000,
427 Invitrogen, A21235). For ChIP-sequencing, the following antibodies were used: anti-

428 H3K27Ac (1:600, Diagonode, C15410196) and anti-H3K27me3 (1:600, Diagonode,
429 C15410195).
430
431 ***Immunoblots of aNSC***
432 aNSC cells were lysed in Laemmli buffer, supplemented with protease (cOmplete; Roche,
433 COEDTAF-RO) and phosphatase (EDTA-free Protease Inhibitor Cocktail; Roche, PHOSS-
434 RO) inhibitors. Proteins were separated by SDS polyacrylamide gel electrophoresis and
435 analyzed by western blotting using standard procedures. After protein transfer, the
436 nitrocellulose membranes (Bio-Rad, catalogue no. 1704271) were blocked by incubation with
437 LICOR Intercept (TBS) blocking buffer. Images were acquired using an Odyssey Imaging
438 System (LICOR).
439
440 ***Imaging of aNSCs***
441 aNSC were fixed with ice-cold methanol for 20 min. Briefly, fixed slides were pretreated with
442 Pepsin (Sigma P-6887), dehydrated and counterstained with DAPI (Thermo, D1306) and
443 mounted with Prolong Diamond Antifade Mounting medium (Thermo, P36965). Images were
444 acquired with a REVOLVE R4 (Echo Laboratories) microscope through a ×63 objective lens.
445 Images were analyzed in the built-in Echo app. Each nucleus was evaluated for the presence
446 of micronuclei and Myc amplification using DNA FISH.
447
448 ***Western immunoblotting***
449 Whole-cell protein lysates were prepared by lysing cells in 10x Cell lysis buffer (Cell signaling)
450 supplemented with cOmplete (Roche) and PhosStop (Roche) phosphatase inhibitors. Protein
451 concentrations were assessed by bicinchoninic acid assay (BCA, Santa Cruz Biotechnology).
452 For 5 minutes, 15 µg of protein was denatured in Laemmli buffer at 90 °C. Samples were run
453 on NuPage 10 % polyacrylamide, 1 mm Tris-Glycine Protein Gels (Thermo Fisher Scientific)
454 and transferred to PVDF membranes (Roche). Membranes were blocked with 5 % dry milk in
455 TBS with 0.1 % (v/v) Tween-20 (Carl Roth). Membranes were probed with primary antibodies
456 overnight at 4 °C and then with secondary antibodies conjugated to horseradish peroxidase for
457 1 hour at room temperature. Chemiluminescent detection of proteins was carried out using
458 Pierce ECL Western blotting substrate (Thermo Fisher) and the ChemiDoc (Bio-Rad).
459 Densitometry was performed using ImageJ (NIH).
460
461 ***Inducible shRNA knock-down plasmid cloning***

462 shRNA constructs were designed using the genetic perturbation platform by the Broad Institute
463 and ordered from Eurofins. They were cloned into pRSITEP-U6Tet-sh-EF1-TetRep-2A-Puro
464 (Celltecta) following the manufacturer's instructions. We generated three independent shRNAs
465 targeting CIP2A (1: TGCGGCACTTGGAGGTAATTT, 2:
466 ATTTGTGACTTCGTAACAATA, 3: GCTAGTAGACAGAGAACATAA), two targeting
467 TOPBP1 (1: GATAGATTTGGGTAGTAATTT, 2: GCTGCAAAGAAGTGGAATTTA), and
468 one targeting MDC1 (1: CGGACCAAACTTAACCAAGAA). Successful insertion was
469 confirmed by full plasmid sequencing (Plasmidsaurus).
470
471 ***Lentivirus production and cell transduction***
472 Lentivirus production was carried out as previously described[37]. In brief, HEK293T cells were
473 transfected with PEI MAX (Polysciences Inc) in a 2:1:1 ratio of the lentiviral vector and
474 psPAX2 and pMD2.G packaging plasmids (Addgene), according to the manufacturer's
475 instructions. Viral supernatant was collected 48 and 72 hours after transfection. The
476 supernatant was pooled, filtered, and stored at –80°C. Cells were transduced with virus
477 particles in the presence of 5 µg/ml polybrene (Merck). Cells were transduced for 1 day in
478 antibiotic-free medium and then grown in full medium for 1 day. Neuroblastoma cells were
479 then selected for 2 days with puromycin hydrochloride (10 µg/ml) or geneticin disulphate
480 (G418, Roth) (2mg/ml). Plasmid expression was induced using 5 µg/ml doxycycline (Sigma-
481 Aldrich Inc., D9891) for 2 days. Western blot validation was done as described above.
482
483 ***Targeted DNA damage induction by CRISPR-cas9***
484 To induce targeted DNA damage on amplicons, which we refer to as a DNA segment that has
485 undergone focal, high-level amplification, in COLO 320DM/HSR, DMS273 cells, we used
486 CRISPR-cas9. CrRNA used in COLO 320DM/HSR was designed to target an intergenic
487 region amplified in both cell lines (sequence: chr8:+127572615:
488 TACAACGAACTATTTAACCG, TGG(pam)). crRNA used in targeting *MYC* containing
489 ecDNA in DMS273 cells was: GGAGAGCTTGTGGACCGAGC. Non-targeting control was
490 also included (IDT, cat: 1072544). Equal amounts of crRNA and tracerRNA were mixed and
491 annealed before mixing with Alt-R™ S.p. Cas9 Nuclease V3, (IDT, cat:1081059) to make the
492 RNP complex. RNP complex was stabilized by incubating at room temperature for 15 minutes,
493 after which it was delivered into cells using electroporation with the Nucleofector system from
494 Lonza, using program CM-138 and solution SF (Lonza, Catalog #: V4XC-2012). After
495 electroporation, cells were immediately seeded onto coverslips previously coated with

496 fibronectin (10 µg/ml). Cells were fixed at the indicated time points and subjected to multiplex
497 immunofluorescence and DNA-FISH staining.
498
499 ***Preparation of metaphase spreads***
500 Cells were grown to 80% confluency in a 15 cm dish and metaphase-arrested by adding
501 KaryoMAX™ Colcemid™ (10 µL/mL, Gibco) for 1-2 hours. Cells were washed with PBS,
502 trypsinized and centrifuged at 200 g for 10 min. We added 10 mL of 0.075 M KCl preheated
503 at 37 °C, one mL at a time and vortexing at maximum speed in between. Afterwards, cells were
504 incubated for 20 min at 37 °C. 5 mL of ice-cold 3:1 MeOH/acetic acid (kept at -20 °C) were
505 added, one mL at a time followed by resuspension of the cells by flicking the tube. The sample
506 was centrifuged at 200 g for 5 min. Addition of the fixative followed by centrifugation was
507 repeated four times. Two drops of cells within 200 µL of MeOH/acetic acid were dropped onto
508 prewarmed slides from a height of 15cm. Slides were incubated overnight.
509
510 ***Fluorescence in situ hybridisation (FISH)***
511 Metaphase spreads or cells seeded on coverslips for interphase FISH were fixed in
512 MeOH/acetic acid for 20 min at -20 °C followed by a PBS wash for 5 min at RT. The wells
513 were removed, and slides were digested in Pepsin solution (0.001 N HCl) with the addition of
514 10 µl pepsin (1 gr/50 mL) at 37°C for 10 min. After a wash in 0.5x SSC for 5 min, slides were
515 dehydrated by washing in 70 %, 90 % and 100 % cold ethanol stored at -20 °C (3 min in each
516 solution). Dried slides were stained with either a 5 µl of Vysis LSI N-MYC
517 SpectrumGreen/CEP 2 SpectrumOrange Probes (Abbott), ZytoLight ® Spec CDK4/CEN12
518 Dual Color Probe (ZytoVision) or ZytoLight ® SPEC MDM2/CEN 12 Dual Color Probe
519 (Zytovision), covered with a coverslip and sealed with rubber cement. Denaturing occurred in
520 a Thermobrite (Abbott) for 5min at 72 °C followed by 37 °C overnight. The slides were washed
521 for 5 min at RT within 2× SSC/0.1 % IGEPAL, followed by 3 min at 60 in 0.4× SSC/0.3 %
522 IGEPAL (Sigma-Aldrich Inc.) and further 3 min in 2× SSC/0.1 % IGEPAL at RT. Dried slides
523 were stained with 12 µl Hoechst 33342 (10 µM, Thermo Fisher) for 10 min and washed with
524 PBS for 5 min. After drying, a coverslip was mounted on the slide and sealed with nail polish.
525 Images were taken using a Leica Stellaris Confocal microscope. For ecDNA copy number
526 estimation, we counted foci using FIJI's find maxima function. Nuclear boundaries were
527 marked as regions of interest. The threshold for signal detection within the regions of interest
528 was determined manually and used for all images analyzed within one group.
529

530 ***Indirect Immunofluorescence (IF)***

531 Cells were fixed in 4% paraformaldehyde (Electron Microscopy Science) prepared in PHEM
532 buffer (Sigma-Aldrich) for 10 minutes at room temperature, with fresh fixative applied after
533 the first 2 minutes. Fixed cells were washed three times in 125 mM glycine/PHEM for 5
534 minutes each, followed by permeabilization with 0.5% Triton X-100 (Sigma-Aldrich) in
535 PHEM for 10 minutes at room temperature. After a single 5-minute wash in PHEM, cells were
536 blocked in 5% fetal calf serum (FCS, Sigma-Aldrich) containing 0.1% Tween-20 (Bio-Rad) in
537 PHEM for 30 minutes at room temperature. Primary antibodies were diluted in 5% FCS/0.1%
538 Tween-20/PHEM and applied to cells overnight at 4 °C. The following day, cells were washed
539 three times in 0.1% Tween-20/PHEM for 10 minutes each and incubated with secondary
540 antibodies diluted in 5% FCS/0.1% Tween-20/PHEM for 2 hours at room temperature. After
541 incubation, cells were washed three additional times in 0.1% Tween-20/PHEM for 10 minutes
542 each. Nuclei were counterstained with 5 µM Hoechst 33342 (Thermo Fisher Scientific) in
543 PHEM for 10 minutes, followed by three washes in PHEM for 5 minutes each. Cells were air-
544 dried for 5 minutes and mounted onto SuperFrost glass slides (Epredia) using 5 µl of ProLong
545 Glass Antifade Mountant (Thermo Fisher Scientific). For double immunofluorescence, both
546 primary and secondary antibodies were applied simultaneously.

547

548 ***Combined FISH and immunofluorescence (ImmunoFISH)***

549 Interphase cells were plated on Poly-D-lysine-coated coverslips (Neuvitro Corporation) in 24-
550 well plates. Cells were fixed with 4% paraformaldehyde for 10 minutes at room temperature,
551 followed by three washes with 125 mM glycine in PBS (5 minutes each). Permeabilization was
552 performed using 0.5% Triton X-100 in PBS for 10 minutes at room temperature, followed by
553 three washes with PBS. Cells were then blocked in 3% bovine serum albumin (BSA) for 30
554 minutes and incubated overnight at 4 °C with the primary antibody diluted in 3% BSA. After
555 three additional PBS washes, cells were incubated with the secondary antibody (diluted in 3%
556 BSA) for 2 hours at room temperature. Post-incubation, cells were re-fixed in 4%
557 paraformaldehyde for 20 minutes at room temperature. DNA was subsequently denatured by
558 treating cells with 0.7% Triton X-100 and 0.1 M HCl on ice, followed by additional chemical
559 denaturation in 1.9 M HCl for 30 minutes at room temperature. The slides were then washed
560 with 125 mM glycine in PBS, followed by a 5-minute wash in 2× saline-sodium citrate (SSC)
561 buffer. Dehydration and probe hybridization was conducted following the standard FISH
562 protocol described above.

563

564 ***Triple FISH***

565 Cells were cultured on poly-D-lysine–coated coverslips (Neuvitro Corporation) placed in 24-
566 well plates and fixed in methanol/acetic acid (3:1, v/v) for 20 min at −20 °C. Coverslips were
567 equilibrated in 2× SSC and subsequently dehydrated through a graded ethanol series (70%,
568 85%, and 100%, 2 min each). For hybridization, 2 µl of each probe specific for *CDK4, MYCN*,
569 and *MDM2* (myTags®, Arbor Biosciences) conjugated to Alexa 488, Atto 550, and Atto 633,
570 respectively, were mixed with 10 µl hybridization buffer (50% formamide, 10% dextran
571 sulfate, 40 ng/µl RNase A in SSCT). A 5 µl aliquot of this mixture was applied per coverslip.
572 Hybridization was carried out at 80 °C for 10 min followed by incubation at 37 °C overnight.
573 Post-hybridization washes were performed according to the standard protocol for single-gene
574 DNA FISH. For ecDNA copy number estimation in triple FISH experiments, foci were
575 detected using Radial Symmetry-FISH (RS-FISH)[38]. Parameters were set manually for each
576 channel and applied to all images from the same coverslip.

577

578 ***Live-cell imaging***

579 Live-cell imaging presented in Extended Fig. 10a was performed as previously described[27].
580 The stably engineered COLO320 DM cell line[27] was used to conduct live-cell imaging. Before
581 cell seeding, 96-well glass-bottom plates were coated using poly-D-lysine. The medium was
582 replenished with FluoroBrite DMEM (Gibco, A1896701), with 10% FBS, 1x GlutaMax and
583 prolong live antifade reagent diluted in 1:200 ratio (Invitrogen, P36975) 30 minutes prior to
584 imaging. The 96-well plate was fitted onto a top stage incubator (Okolab) and imaged on a
585 Leica DMi8 widefield microscope using a x63 oil objective. Temperature (37˚C), humidity and
586 CO2 (5%) were stably maintained throughout the experiment.

587

588 ***Micronuclei-harbouring cell fitness analysis via live-cell imaging***

589 COLO 320DM-Tg19 cells were seeded in a coated well of a 96-well glass-bottom plate and
590 treated with 50 µM hydroxyurea to enrich micronuclei formation. After 24 hours, hydroxyurea
591 was removed and replaced with FluoroBrite DMEM (Gibco, A1896701), with 10% FBS, 1x
592 GlutaMax and prolong live antifade reagent diluted in 1:200 ratio (Invitrogen, P36975). Z-
593 stack images were acquired every 3 hours for a total of 60 to 72 hours, and images were
594 processed using Small Volume Computational Clearing. Maximum Intensity projections were
595 made on cropped frames of daughter cells immediately after initial division and for which at
596 least one daughter cell contained a micronucleus. The micronucleus amplicon status (presence
597 or absence of ecDNA$^+$ or ecDNA-negative micronuclei) and micronucleus size (denoted as

598 large if diameter is greater than 2 µm) of each daughter cell were recorded. The fate of daughter
599 cells was manually tracked and assigned to the following three categories: continued division,
600 cell death, or remaining undivided for the 72h imaging period. If the daughter cell divided, the
601 timepoint at which the next division occurred was recorded to quantify time to next division
602 (T2D). Cropped maximum intensity projections were imported into Aivia (v.12.0.0). Outlines
603 were manually drawn around primary nuclei and their corresponding micronuclei. A machine
604 learning-based pixel classifier and recipe were used to identify TetR-mNeonGreen foci by
605 which ecDNA copy number in the primary nuclei and micronuclei were quantified. EcDNA
606 status of micronuclei was classified as high or low relative to the median ecDNA content within
607 micronuclei among all micronuclei.
608
609 ***Microscopy, image acquisition and analysis***
610 All images were acquired using a Leica Stellaris 8 confocal microscope at the Advanced Light
611 Microscopy Technology Platform (Max Delbrück Center for Molecular Medicine). The system
612 was equipped with an HC PL APO CS2 63×/1.40 OIL objective lens and used an immersion
613 oil medium with a refractive index of 1.5185.
614 For imaging individual anaphase cells, the acquisition settings were as follows: 512 × 512
615 pixels frame size, 6× zoom, 0.79 µs pixel dwell time, and a final pixel size of 0.06 µm × 0.06
616 µm. Z-sampling was set to 0.23 µm to capture the entire cell in three dimensions.
617 For groups of interphase cells, images were acquired with a 2048 × 2048 pixels frame size, 2×
618 zoom, 3.16 µs pixel dwell time, and a final pixel size of 0.05 µm × 0.05 µm.
619 Fluorophores were excited using diode laser lines at 561 nm (Alexa Fluor 568), 488 nm (Alexa
620 Fluor 488), and 405 nm (Hoechst). Fluorescence emissions were detected at 566–620 nm
621 (Alexa Fluor 568), 500–550 nm (Alexa 488), and 420–480 nm (Hoechst) using a pinhole set
622 to 1 Airy unit (AU).
623 To ensure comparability across samples, all images were acquired under identical instrument
624 settings.
625 The "Find Maxima" function was employed to quantify extrachromosomal DNA (ecDNA)
626 copy numbers in FISH images. In anaphase cells, lagging DNA was defined as chromosomal
627 material visibly separated from the primary segregating chromosomes by a minimum distance
628 of 0.3 µm across the Z-stack, consistent with the lateral resolution limit of the imaging system.
629 Images for Extended Fig 3b-d 3f, / Extended Fig. 8b were taken by a ZEISS LSM 880 inverted
630 confocal microscope using ZEN (black v.2.3), and images for Fig 2bm, 2i-j, Extended Fig. 2d-
631 f, 3h-i, Extended Fig. 8h-i were taken by a Leica DMi8 widefield microscope by Las X

632 software (v.3.8.2.27713) using a ×63 oil objective. Z-stacks were taken for each field of view
633 with image pre-processed using Small Volume Computational Clearing, and a max projection
634 was performed by ImageJ (v.1.53t) before proceeding for further image analysis. Individual
635 splitted channel images were semi-automatically segmented and analyzed by CellProfiler
636 (v.4.2.1). Micronuclei were scored manually and defined as round structures separated from
637 the primary nucleus, with a diameter up to one third of the size of the main nucleus, as
638 previously described[25,39].
639 Colocalization analysis was done using Huygens software (deconvolution, v24.10), FIJI (tile
640 stitching, v2.14) and Imaris (colocalization analysis, v10.2).
641
642 ***Nanopore-based replication fork dynamics***
643 CHP212-PIP-FUCCI cells were seeded into T-300 flasks without Hygromycin B. At 70%
644 confluency, cells were treated with or without 80 µM hydroxyurea for 24h. CHP212-PIP-
645 FUCCI cells were then successively treated with 50 µM EdU for 3 minutes, 50 µM BrdU for 6
646 minutes, 100 µM Thymidine for 20 minutes, with 3 PBS washes in between each step. 80 µM
647 hydroxyurea was maintained during the whole time, if treated. Cells were trypsinized, washed
648 with PBS and sorted for S-phase (mCherry+, mVenus−) using a BD FACSAria Fusion. Sorted
649 cells were pelleted, flash frozen in liquid nitrogen and stored at -80°C until DNA extraction.
650 High molecular weight DNA was extracted using the NEB Monarch HMW DNA Extraction
651 Kit for Tissue (NEB, T3060). DNA libraries for nanopore sequencing were prepared using the
652 Ultra-Long DNA sequencing KIT (ONT, SQK-ULK001) according to the manufacturer's
653 instructions. Libraries were sequenced on R9.4.1 flow cells on the MinION platform.
654 Reads were basecalled using Guppy (v6.4.6, dna_r9.4.1_450bps_hac model, ONT) and aligned
655 to hg38 using minimap2[40] (v2.30). We used DNAscent (v3.1.2)[41] to investigate replication fork
656 dynamics. We applied the DNAscent detect function to detect EdU and BrdU incorporation on
657 nanopore reads in batches of around 4000 reads. The forkSense function was then used to
658 classify replication forks based on the order EdU and BrdU incorporation.
659 To determine replication fork speeds, we only retained complete forks (forks running off the
660 end of a read were excluded) from the forkSense output. We then overlapped the remaining
661 forks with the Decoil amplicon reconstruction for CHP212 and classified them as either
662 circular (overlapping with ecDNA regions) or linear (overlapping with any other region). To
663 compare ecDNA forks with linear forks of similar chromatin context, we further filtered forks
664 which overlapped with active regions, by H3K27ac ChIPseq peaks. Bed files for peak calls
665 were taken from[42] and downloaded from GEO (GSE90683) and converted from hg19 to

666 hg3838 using the UCSC liftover tool (https://github.com/ucscGenomeBrowser/kent). Fork
667 speeds were calculated by dividing the length of each detected fork by the treatment time
668 beginning with the start EdU treatment until the start of the thymidine chase out (Untreated: 15
669 min; HU: 16.4 min).
670
671 ***Laser-microdissection and Whole Genome Amplification (WGA) of single (micro-)nuclei***
672 TR-14 cells were directly grown on Poly-D-Lysine coated (Gibco, A3890401) PEN-membrane
673 metal frame slides (Leica, 11600289). Immunofluorescence was performed as described above.
674 Slides were stored in 1x PHEM in the dark at 4°C until dissection. Single micronuclei, pooled
675 micronuclei (5-10 micronuclei) and single primary nuclei were manually visualised and
676 identified on a Leica microdissection microscope (LMD7 or LMD7000, Leica microsystems).
677 We collected primary nuclei and micronuclei from independent cells and primary and
678 micronuclei from the same cell in a subset of samples (Extended Fig. 9d). Shapes were
679 collected into adhesive PCR caps (MicroDissect GmbH, MDCA8W1K20). WGA was
680 performed as in the ImmunoGAM method, with minor modification[43,44]. Sequencing libraries
681 were prepared using the NEBNext Ultra II FS (New England Biolabs, E7805) kit according to
682 the manufacturer's protocol with reduced reaction volumes (1/4). Samples were barcoded for
683 Illumina sequencing using the NEBNext Multiplex Oligos for Illumina kit (New England
684 Biolabs, E7874) and sequenced on a NextSeq2000 sequencer (Illumina) or Novaseq X
685 (Illumina) in 2×150-nt or 2 x 100-nt paired-end mode.
686
687 ***Amplicon reconstruction in TR-14***
688 Four distinct ecDNA elements were reconstructed for TR14 using Decoil[33] 1.1.2 with
689 parameters –min-vaf 0.1 –min-cov-alt 10 –min-cov 8 –fragmentmin-cov 10 –fragment-min-
690 size 1000 –filter-score 35 or –min-vaf 0.01 –min-cov-alt 10 –min-cov 10 –max-explog-
691 threshold 0.01 –fragment-min-cov 10 –fragment-min-size 500, with the reference genome
692 GRCh38/hg38 and annotation GENCODE V42, (as in[33]). Additionally, a de novo assembly
693 contig containing CDK4 for TR14 was assembled using Shasta[45] (v0.6.0) with adjusted
694 parameters minReadLength = 10000, k = 14, consensus caller
695 Bayesian:SimpleBayesianConsensusCaller-10.csv. The contig was aligned to GRCh38/hg38
696 using minimap2[40] with parameters -x asm10. From the PAF alignment the overlapping
697 genomic coordinates were extracted as BED file. Using the genomic regions of all amplicons
698 found in TR14 a BED file and a custom reference genome was computed, which includes (1)

699 a masked GRCh38/hg38 genome of the regions overlapping the amplicons and (2) the FASTA
700 sequence of all the ecDNA elements as additional contigs.
701
702 ***Identification of micronucleated sequences***
703 Reads were quality and adapter-trimmed using Trim Galore[46] (v0.6.10) and aligned to the
704 human reference assembly GRCh38 with added EBV contig (NC_007605.1) using BWA-
705 MEM[47] (v 0.7.18) with default parameters. Duplicate reads were removed using Picard[48]
706 (v3.3.0) MarkDuplicates. We collected all samples over a total of 2 experiments which were
707 sequenced on different flowcells. Samples from the run with higher sequencing depth were
708 downsampled to match the median number unique reads from the other run using samtools
709 view with the -s parameter. BigWig files were generated using Deeptools2[49] (v3.5.5)
710 bamCoverage with a binsize of 25kb and CPM normalization.
711
712 ***Candidate window identification***
713 For each sample, we identify candidate windows, which represent genomic regions covered by
714 reads significantly over background, detected by performing the following 4-steps: (1) The
715 genome was divided into 25kb bins and the number of reads and number of bases covered by
716 at least one read were counted with bedtools coverage. (2) For each sample, we fitted a negative
717 binomial distribution on the per-bin read counts, similar to[50]. Distribution parameters were
718 estimated using Maximum Likelihood Estimation as implemented in the fitdistrplus[51] (v1.2.1)
719 R-Package. The threshold RC_{th} for per-bin read counts was derived from the first read count
720 value of the cumulative mass function, where the probability of it being larger than threshold
721 RC_{th} was <0.001, as defined as >1-P, where P denotes the probability of a value being less or
722 equal than threshold RC_{th}. (3) To remove bins with focal read accumulation, thus being bins
723 with high read counts but low coverage, we further sorted all bins based on the percentage of
724 bases covered. We defined a coverage threshold C_{th} as the 99th percentile. (4) Only bins with
725 a read count > RC_{th} and coverage > C_{th} where retained as candidate windows.
726 To identify enriched sequences under the assumption that DNA sequestered into micronuclei,
727 which are detectable by light microscopy, derive from chromosomes, chromosomal fragments
728 or other longer chromosomal units (such as ecDNA) of a certain length, we further refine the
729 candidate window set by removal of solidary windows, which adhere to the candidate window
730 definition as described above, but do not have any adjacent candidate windows or are of small
731 size. With this approach we limit the smallest detectable unit size, but make sure to further
732 remove regions, which are most likely derived from amplification and/or mapping noise.

733 We pivot through each candidate window and search for adjacent candidate windows up and
734 downstream within a radius r. A radius of r=4 was used in this study. If a candidate window
735 has at least one other candidate window upstream and downstream within the radius r, this
736 candidate window is further classified as a body segment, while candidate windows with only
737 at least one other candidate window within the radius r on either side, are classified as edge
738 segment. If a candidate window does not have any other candidate windows within its radius,
739 this window is removed from analysis. We further align edge and body segments into closed
740 segments, where body segments must be flanked by edge segments to be retained, thus making
741 an edge-body-edge alignment the smallest detectable unit, which for this experiment is a
742 fragment size of 75kb. If an edge segment is flanked by another edge segment, both windows
743 are removed from further analysis.
744
745 ***Copy number calling***
746 Copy number profiles for each sample were computed similarly to CNVkit[52] using a custom
747 python script utilizing the Pysam API (https://github.com/pysam-developers/pysam). First, the
748 genome was tiled into 500kb bins. For each bin, per base coverages were summed up and
749 divided by the bin size to get a per bin mean coverage, which was then log2 transformed.
750 Visualization and segmentation of copy number profiles were computed using a custom R
751 script (https://github.com/henssen-lab/ecMN/tree/main/copy_number). First, only canonical
752 chromosomes (autosomes and sex chromosomes) were retained and telomeric and centromeric
753 regions filtered out. GC content for each bin was calculated using the R package Biostrings[53].
754 We performed GC correction for the log2 per bin mean coverage values using the loess function
755 from the stats R-package with a smoothing span of 0.3 and performed median centering based
756 on all autosomal bins. Segmentation was performed using circular binary segmentation, as
757 implemented in the DNAcopy[54] R-package. After smoothing and outlier removal using the
758 smooth.CNA function, segments were called using the segment function with following
759 parameters: undo.splits = "sdundo", undo.SD = 1.5. Log2 per bin coverages and segments were
760 visualized with ggplot2[55].
761
762 ***(Micro-)nuclear sequence analysis***
763 ***Quality control and filtering***
764 Single and pooled micronuclei samples were retained for downstream analysis if they
765 contained more than 20 called windows and >100000 uniquely mapping reads. We additionally
766 added a second quality control layer, where we inspected the copy number profiles and

767 excluded samples, which showed high degrees of background amplification. Primary nuclei
768 samples were retained if they had more than 50 called windows.
769
770 ***EcDNA consensus sequence calling in single micronuclei***
771 After visual inspection of called regions in single micronuclei, we observed an enrichment of
772 sequences overlapping the amplicon regions, as described above. To identify the consensus
773 region between enriched sequences in single micronuclei and ecDNA reconstructions for
774 further quantification, we generated a set of all called windows from single micronuclei passing
775 quality control. We retained each genomic region, which was called in at least 2 samples. We
776 overlapped these regions with the custom reconstructions and were able to retain the majority
777 of ecDNA regions in single micronuclei. The only region we could not capture was a short
778 region in chromosome 1, whose length fell below the smallest detectable unit size of 75kb as
779 described above. The consensus ecDNA regions were used for subsequent analysis.
780
781 ***Circular read enrichment estimation (log2 coverage)***
782 To quantify read enrichment over the consensus ecDNA regions, we further normalized the
783 absolute per-bin read counts to counts per million to account for different library size. To
784 estimate the enrichment of circular reads, we divided the mean coverage of all consensus
785 ecDNA regions by the winsorized mean coverage (top and bottom 5% values replaced) of all
786 non-ecDNA regions, as implemented in the Winsorize function from the R-Package
787 DescTools[56] (v0.99.58). The coverage ratio was further log2 transformed.
788 To quantify the signal over each connected consensus ecDNA region over their flanking region,
789 we obtained region-scaled coverage values using Deeptools2 computeMatrix scale-regions
790 with parameters: -m 250000 -b 125000 -a 125000 -bs 25000 –missingDataAsZero –
791 outFileNameMatrix.
792
793 ***Co-segregation and relative ecDNA fraction analysis***
794 To assess ecDNA co-segregation heterogeneity, we counted the presence or absence for each
795 amplicon in all single micronuclei and primary nuclei samples. For each sample, we overlapped
796 all called windows with the amplicon reconstructions. An amplicon was deemed present, if it
797 had at least 1 overlapping called window.
798 To evaluate the relative copy number differences between different amplicons within one
799 sample we computed amplicon fractions within all circular reads. Read counts for each
800 amplicon were first divided by its respective amplicon length to normalize counts for amplicon

801 size. The length normalized counts for each amplicon were further divided by the sum of the
802 length normalized counts of all amplicons to obtain a value, which represents the fraction of
803 reads belonging to each respective amplicon within all circular reads.
804
805 ***Linear chromatin enrichment analysis***
806 To identify chromosomal fragments, which are enriched in single micronuclei, we first
807 accumulated per chromosome read counts, excluding all reads mapping to the amplicon
808 regions, and normalised them to chromosome size. Enriched chromosomes have high read
809 accumulation over background mapping. We therefore identified enriched chromosomes as
810 extreme outliers, if the normalised read count was larger than: Q3 (3rd quartile) + 10 * IQR
811 (interquartile range). The fragment length of the enriched chromosome was determined by
812 summing up the number of bins, where the per bin read count was larger than the 90th percentile
813 of all non-zero bins within the identified enriched chromosome.
814
815 ***Chromatin immunoprecipitation (ChIP)-sequencing***
816 Hydroxyurea- and DMSO-treated COLO320DM cells were washed 2x with prewarmed 1X
817 PBS. Cells were fixed by addition of 10mL ice-cold 1% FA in 10% FCS-RPMI-1640 and
818 incubated for 10 min on a shaker. The fixation reaction was quenched by addition of 550uL
819 ice-cold 2.5M Glycine in PBS. Cells were washed 1x with ice-cold 1X PBS before scraping
820 down in 10 mL ice-cold 1X PBS. Fixed cells were centrifuged at 500 x g for 5 min at 4°C and
821 resuspended in ice-cold 1X PBS for a total of 2 washes. Cells were pelleted and snap frozen in
822 liquid nitrogen and stored at -80 C for no more than 1 week.
823 Cell pellets were resuspended in 5 mL ice-cold lysis buffer 1 (140 mM NaCl; 50 mM HEPES-
824 KOH pH 7.5; 1 mM EDTA; 10% Glycerol (v/v); 0.5% IGEPAL CA-630 (v/v); 0.25% Triton
825 X-100 (v/v); 1x Protease inhibitor (Roche, 04693132001)) and incubated on a roller at 4°C for
826 10 min. Lysed cells were centrifuged at 1357 x g for 5 min, resuspended in 4 mL lysis buffer
827 2 (20 mM NaCl; 10 mM Tris-HCl pH 8.0; 2 mM EDTA; 0.5M EGTA; 1x Protease inhibitor)
828 and incubated on a roller for 10 min at room temperature. The lysate was centrifuged at 1357
829 x g for 5 min at 4°C and resuspended in 900 µL sonication buffer (100 mM NaCl; 10 mM Tris-
830 HCl pH 8; 1 mM EDTA; 0.5 EGTA; 0.1% Na-deoxycholat (w/v); 0.5% N-Laroylsarcosine
831 (w/v); 1x Protease inhibitor). Lysed chromatin was sheared to a fragment size of 200-500 base
832 pairs (bp) on a Covaris S220 (PIP 140, DF 5, CPB 200) for 12 min. Sheared chromatin was
833 clarified by addition of 1/10 volume 10% Triton X-100 (v/v) and centrifugation at maximum
834 speed at 4°C.

835 Protein-DNA-complexes were immunoprecipitated by overnight incubation with the
836 respective primary antibody on a rotator at 4°C. 10-15 µg total chromatin was used per sample.
837 30 µL Protein G beads (Invitrogen, 10003D) were washed 3x in 0.25% BSA in PBS (w/v) and
838 added to each sample. Samples were incubated overnight on a rotator at 4°C.
839 Antibody-bead - complexes were washed in RIPA buffer (50 mM HEPES-KOH pH 7.5; 1mM
840 EDTA; 1% IGEPAL CA-630 (v/v); 0.7% Na-deoxycholat (w/v); 500 mM LiCl; 1x Protease
841 inhibitor) for a total of 7 times followed by 1 wash in TE buffer (10 mM Tris-HCl pH 8.0;
842 1mM EDTA; 50 mM NaCl; 1x Protease inhibitor). Beads were eluted in 200 µL Elution Buffer
843 (50 mM Tris-HCl pH 8.0; 10 mM EDTA, 1% SDS (v/v)). 20 µL 5M NaCl and 5 µL Proteinase
844 K (NEB, P8107S) were added to each sample and DNA was de-crosslinked at 65°C overnight,
845 followed by RNA digestion with 2 uL RNase A (Invitrogen, R1253) at 37°C for 30 minutes.
846 DNA was purified using the QIAquick PCR Purification Kit (Qiagen, 28104) according to the
847 manufacturer's instructions. ChIP DNA libraries were constructed using the NEBNext Ultra II
848 DNA Library Prep Kit (NEB, E7645S) and barcoded for Illumina sequencing using the
849 NEBNext Multiplex Oligos for Illumina kit (NEB, E7780S). Libraries were sequenced on a
850 NovaSeq X Plus sequencer (Illumina) in 100 nt single-end mode.
851
852 ***ChIP-sequencing analysis***
853 The raw reads were quality and adapter-trimmed using Trim Galore and aligned to the human
854 reference assembly GRCh38 with an added EBV contig (NC_007605.1) using BWA-MEM
855 with default parameters. Duplicate reads were removed using Picard MarkDuplicates. Library
856 quality was assessed using strand cross-correlation metrics (RSC and NSC) from
857 Phamtompeakqualtools[57,58] (v1.2.2).
858 Using the deduplicated BAM file, read densities per 10 bp window were generated using
859 DeepTools2 bamCoverage. Genomic bins overlapping the ENCODE DAC blacklist regions
860 were filtered out using the parameters: --ignoreForNormalization chrX chrM NC_007605.1 --
861 scaleFactor 10 --effectiveGenomeSize 2805636231 --exactScaling --extendReads 200 --
862 normalizeUsing CPM and input-substracted using the bigwigCompare function.
863
864 ***RNA-sequencing***
865 Three replicates of Hydroxyurea- and DMSO-treated COLO320DM cells were washed with
866 1x PBS, trypsinized (Gibco) and centrifuged at 300xg for 5 min. Total RNA was immediately
867 extracted from the cell pellets using the RNeasy Mini Kit (Qiagen, 74104) following the
868 manufacturer's instructions. Genomic DNA was removed by DNase treatment using the

869 RNase-Free DNase Set (Qiagen,79254). The mRNA library was constructed using the TruSeq
870 Stranded mRNA Library Prep kit (Illumina) at the Berlin Institute of Health (BIH) Genomics
871 Technology Platform. Libraries were sequenced on a NovaSeq X Plus sequencer (Illumina) in
872 100 nt single-end mode.
873
874 ***RNA-sequencing analysis***
875 Reads were quality and adapter-trimmed using Trim Galore and aligned to the human reference
876 assembly GRCh38 with an added EBV contig (NC_007605.1) using STAR[59] (v2.7.11b) with
877 parameters --twopassMode Basic --outSAMtype BAM SortedByCoordinate. Reads were
878 counted per gene against GENCODE gene annotation (Release 47) using htseq[60] (v2.0.5)
879 htseq-count with parameters -r pos -s no. Counts were normalized for library size and
880 composition using sizefactors from DEseq2[61] (v1.38.3). Counts were z-score normalized for
881 visualization using the scale function in R-base (v4.2.2). Differentially expressed genes
882 between the untreated and treated samples were identified using DEseq2 and p-values were
883 corrected for multiple testing using the Benjamini-Hochberg procedure. Gene set enrichment
884 analysis was performed on differentially expressed genes with an adjusted p-value <0.05
885 against MSigDB hallmark gene sets using the GSEA function in Clusterprofiler[62] (v4.6.2) and
886 visualized with DOSE[63] (v3.24.2).
887
888 ***Patient samples and clinical data access***
889 This study comprised the analyses of tumour and blood samples of patients diagnosed with
890 neuroblastoma between 1991 and 2022. Patients were registered and treated according to the
891 trial protocols of the German Society of Pediatric Oncology and Hematology (GPOH). This
892 study was conducted in accordance with the World Medical Association Declaration of
893 Helsinki (2013) and good clinical practice; informed consent was obtained from all patients or
894 their guardians. The collection and use of patient specimens and clinical data was approved by
895 the institutional review boards of Charité-Universitätsmedizin Berlin and the Medical Faculty,
896 University of Cologne. Specimens and clinical data were archived and made available by
897 Charité-Universitätsmedizin Berlin or the National Neuroblastoma Biobank and
898 Neuroblastoma Trial Registry (University Children's Hospital Cologne) of the GPOH. The
899 *MYCN* copy number was determined as a routine diagnostic method using FISH. DNA and
900 total RNA were isolated from tumour samples with at least 60% tumour cell content as
901 evaluated by a pathologist.
902

903 ***Clinical data analysis***

904 Patients were registered in the GPOH trials NB90[64], NB97[65], NB2004 (NCT00410631) and
905 NB2016-registry. All protocols were approved by the ethics committees of the Universities of
906 Cologne as leading institutions (see supplemental table 2 for approval numbers), and approval
907 was confirmed by the local ethics committees. Informed consent was obtained from the
908 participants at the local treatment site and was a prerequisite to register in the respective trials.
909 Trial participation was a requirement for inclusion in this analysis. For the purpose of this
910 analysis, follow-up information was evaluated for matching tumour samples of a respective
911 patient. The endpoints were overall and event-free survival. Overall survival (OS) was defined
912 as death of any cause and event-free survival (EFS) was defined as disease progression or
913 relapse, or death of any cause. Patients without event were censored at last follow-up. OS and
914 EFS were calculated using the Kaplan-Meier estimator[66]. The log rank test was used for
915 comparison. A Cox proportional hazards regression was conducted for ecDNA+ micronuclei
916 percentage. Statistical analysis was conducted using SPSS 29 (Armonk, New York, U.S.).
917 Despite availability, exclusively clinical data of samples collected at first diagnoses before the
918 start of therapy were included to eliminate a potential bias due to therapy-related changes of
919 tumour genetics.

920

921 ***Modelling of ecDNA segregation patterns***

922 ***Estimation of ecDNA mis-segregation probability***

923 To estimate the mis-segregation probability of ecDNA in a patient or cell line, we adapted a
924 binomial model of micronucleation[67]. According to this model, the frequency of cells without
925 micronuclei is given by $P_0(p_{MN}, C) = (1 - \frac{1}{2}p_{MN})^C$, where pMN is the mis-segregation
926 probability of an ecDNA element during cell division and C is the amount of ecDNA elements
927 in the cells. Per patient and cell line where we have more than five cells imaged, we then use
928 the average observed ecDNA copy number by FISH per cell and frequency of non-
929 micronucleated cells to calculate p_{MN}.

930

931

932 ***Biased Random Segregation Model***

933 We developed a model to simulate ecDNA segregation during cell division. A single cell
934 begins with a random ecDNA copy number n , sampled from a uniform distribution. Prior to
935 cell division, ecDNA is amplified to $2n$ copies, which are then partitioned between two

936 daughter cells. For cells undergoing random segregation, ecDNA partitioning follows a
937 binomial distribution $B(2n, p_2)$, where $p_2 = 0.5$. In contrast, for cells exhibiting biased
938 random segregation, partitioning follows a binomial distribution $B(2n, p_1)$, where $p_1 < 0.5$
939 reflects asymmetric segregation. The probability of biased segregation is denoted as q, while
940 $1 - q$ represents the probability of random segregation. The ecDNA copy numbers in the two
941 daughter cells are denoted as n_1 and $n_2 = 2n - n_1$, respectively. The ecDNA fractions f_1
942 and f_2 of the two daughter cells can be calculated as: $f_1 = \frac{n_1}{2n}$, $f_2 = \frac{n_2}{2n}$. By repeating this
943 process, we generate the distribution of ecDNA fractions across daughter cells.
944
945 ***Reconstructing ecDNA Segregation Distribution under Finite Sampling***
946 We first simulated ecDNA segregation in 10^7 cells to establish the "true" or "full"
947 distribution. We then sampled subsets of cells at sample sizes of 10, 25, 50, 100, and 500,
948 repeating each sampling 10^5 times. To quantify the deviation between sampled and true
949 distributions, we calculated the Kolmogorov distances.
950
951 ***Parameter Estimation Using Approximate Bayesian Computation (ABC)***
952 We applied Approximate Bayesian Computation (ABC) to infer the parameters p_1 and q in
953 the model. For the simulated data, 50 pairs of daughter cells were randomly drawn using
954 predefined parameters. During inference, p_1 and q were sampled from prior uniform
955 distributions: $p_1 \sim U(0, 0.5)$ and $q \sim U(0, 1)$. 50 parent cells were randomly selected, with
956 their ecDNA copy numbers drawn from a uniform distribution $U(10, 100)$. For each set of
957 parameters, we ran the model to obtain the ecDNA segregation fraction distribution. To
958 compare the similarity between simulated and target distributions, we computed the
959 Wasserstein distance. A threshold was applied to determine acceptance, generating the
960 posterior distributions of p_1 and q. For experimental data, the same procedure was followed,
961 with the sample size adjusted according to the specific experimental conditions.
962
963 ***Statistical analysis***
964 All experiments were performed a minimum of two times with a minimum of three independent
965 measurements unless otherwise stated. All statistical analysis was performed with R 3.6, R 4.0
966 or Python 3.7. All data are represented as mean ± standard error and tested for normal
967 distribution. Statistical significance was defined as *, $P < 0.05$; **, $P < 0.01$, ***, $P < 0.001$,
968 ****, $P < 0.0001$. Normality was assessed using the Shapiro-Wilk test.

Data availability

Sequencing data produced in this study will be deposited in the European Nucleotide Archive (https://www.ebi.ac.uk/ena/browser/submit). Custom TR14 amplicon reconstructions and FASTA will be available under github.com/henssen-lab. The data that support the findings of this study are available from the corresponding author upon request.

Code availability

Scripts for data analysis within the scope of this publication will be available under https://github.com/henssen-lab/ecMN.

AI assisted copy editing

All text was written by the authors. Parts of the text were copy edited using ChatGPT to improve readability and clarity.

Materials & Correspondence

Correspondence and requests for materials should be addressed to henssenlab@gmail.com

Author Contributions

L.B., R.X., J.T., A.G., A.H., I.T.W., and S.Z., contributed to the study design and collection and interpretation of the data and wrote the manuscript. F.T, M.P, K.P., O.S., J.S., Q.Y., D.P., M.I., A.K., S.H., M.G., A.S.H., M.F., F.B., V.R.L., C.D., X.Y., D.G., S.K., D.G., M.R. N.W., G.M. N.W., performed the experiments, analyzed data and reviewed this manuscript. J.T., I.T.L.W., S.Z., performed the experiments, analyzed and interpreted the data, and edited the manuscript. D.T., A.L., F.D. and M.F. provided data. B.P. and A.H. established essential methods. M.S. analysed the clinical data. R.L., G.B. Y.L., V.B., G.W., R.M., S.P., B.S., A.P., R.P.K., W.H., and B.W. contributed to study design. A.G.H., P.S.M., H.Y.C. led the study design, to which all authors contributed.

Acknowledgements

This work was delivered as part of the eDyNAmiC team supported by the Cancer Grand Challenges partnership funded by Cancer Research UK and led by P.S.M. (CGCATF-2021/100017) (A.G.H.), (CGCATF-2021/100012) (P.S.M. and H.Y.C.), (CGCATF-2021/100020) (B.W and W.H), (CGCATF-2021/100025) (V.B.), and the National Cancer

Institute (OT2CA278644) (A.G.H.), (OT2CA278688) (P.S.M. and H.Y.C.), (OT2CA278670) (B.W and W.H), (OT2CA278635) (V.B.), A.G.H. is supported by the *Deutsche Krebshilfe* (German Cancer Aid) Mildred Scheel Professorship program – 70114107. This project has received funding from the European Research Council (ERC) under the European Union's Horizon 2020 research and innovation programme (grant agreement No. 949172). This project was supported by Cancer Research UK and the National Institute of Health (398299703, the eDynamic Cancer Grand Challenge). Research in the G.B. laboratory is supported by the UK Dementia Research Institute, which receives contributions from the Medical Research Council, UK and the CHDI Foundation, USA. Research at TINS is supported by Romanian PNRR-HUNTGEN-C9-I8 - Contract no. 760114/2023, financed by the European Union – NextGenerationEU. R.X. was supported by the Deutsche Forschungsgemeinschaft (DFG, German Research Foundation) funded Research Training Group (RTG) 2424/CompCancer – project number: 377984878. Work by D.P. in the Andrea Venturas. group was supported by grants from NIH-NCI (P30 CA008748) and (R01 CA282913 to AV), the American Cancer Society Discovery Boost grant (AV), the The Mark Foundation for Cancer Research ASPIRE grant (AV) and by a rapid response grant from the Functional Genomics Initiative (AV). D.P. was supported by an AIRC fellowship for Abroad. The authors want to thank Steven Whittaker for providing important conceptual input. B.W. is supported by a Barts Charity Lectureship (grant no. MGU045) and a UKRI Future Leaders Fellowship (grant no. MR/V02342X/1). W.H is also supported by NNSF General Program (grant no. 3217024. We thank B. Hero, H. Düren, N. Hemstedt of the Neuroblastoma Biobank and Neuroblastoma Trial Registry (University Children's Hospital Cologne) of the German Society of Pediatric Oncology and Hematology (GPOH) for providing samples and clinical data. We thank Sabine Taschner at the St. Anna Kinderkrebsforschungsinstitut for providing cell lines. We thank Andrea Ventura at MSKCC for the establishment and data of the engineered mouse model. Computation has been performed on the HPC for Research cluster of the Berlin Institute of Health. R.P.K. is a Visiting Professor funded by the Stiftung Charité. We thank Hans-Peter Rahn at the MDC Flow Cytometry for support with FACS. Images were acquired at the Advanced Light Microscopy facility of the Max Delbrück Center for Molecular Medicine and the Systems Imaging Facility of the Berlin Institute for Medical Systems Biology.

References

1 Kim, H. *et al.* Mapping extrachromosomal DNA amplifications during cancer progression. *Nat Genet* (2024). https://doi.org:10.1038/s41588-024-01949-7

2 Yi, E., Chamorro Gonzalez, R., Henssen, A. G. & Verhaak, R. G. W. Extrachromosomal DNA amplifications in cancer. *Nat Rev Genet* **23**, 760-771 (2022). https://doi.org:10.1038/s41576-022-00521-5

3 Kim, H. *et al.* Extrachromosomal DNA is associated with oncogene amplification and poor outcome across multiple cancers. *Nat Genet* **52**, 891-897 (2020). https://doi.org:10.1038/s41588-020-0678-2

4 Hung, K. L. *et al.* Targeted profiling of human extrachromosomal DNA by CRISPR-CATCH. *Nature Genetics* **54**, 1746-1754 (2022). https://doi.org:10.1038/s41588-022-01190-0

5 Morton, A. R. *et al.* Functional Enhancers Shape Extrachromosomal Oncogene Amplifications. *Cell* **179**, 1330-1341 e1313 (2019). https://doi.org:10.1016/j.cell.2019.10.039

6 Helmsauer, K. *et al.* Enhancer hijacking determines extrachromosomal circular MYCN amplicon architecture in neuroblastoma. *Nat Commun* **11**, 5823 (2020). https://doi.org:10.1038/s41467-020-19452-y

7 Bailey, C. *et al.* Origins and impact of extrachromosomal DNA. *Nature* **635**, 193-200 (2024). https://doi.org:10.1038/s41586-024-08107-3

8 Chamorro González, R. *et al.* Parallel sequencing of extrachromosomal circular DNAs and transcriptomes in single cancer cells. *Nature Genetics* **55**, 880-890 (2023). https://doi.org:10.1038/s41588-023-01386-y

9 Koche, R. P. *et al.* Extrachromosomal circular DNA drives oncogenic genome remodeling in neuroblastoma. *Nat Genet* **52**, 29-34 (2020). https://doi.org:10.1038/s41588-019-0547-z

10 Wang, Y. *et al.* eccDNAs are apoptotic products with high innate immunostimulatory activity. *Nature* **599**, 308-314 (2021). https://doi.org:10.1038/s41586-021-04009-w

11 Lange, J. T. *et al.* The evolutionary dynamics of extrachromosomal DNA in human cancers. *Nat Genet* **54**, 1527-1533 (2022). https://doi.org:10.1038/s41588-022-01177-x

12 Levan, A. & Levan, G. Have double minutes functioning centromeres? *Hereditas* **88**, 81-92 (1978). https://doi.org:10.1111/j.1601-5223.1978.tb01606.x

13 Kanda, T., Otter, M. & Wahl, G. M. Mitotic segregation of viral and cellular acentric extrachromosomal molecules by chromosome tethering. *J Cell Sci* **114**, 49-58 (2001). https://doi.org:10.1242/jcs.114.1.49

14 Sankar, V. *et al.* Genetic elements promote retention of extrachromosomal DNA in cancer cells. *Nature* (2025). https://doi.org:10.1038/s41586-025-09764-8

15 Di Bona, M. & Bakhoum, S. F. Micronuclei and Cancer. *Cancer Discov* **14**, 214-226 (2024). https://doi.org:10.1158/2159-8290.CD-23-1073

16 Terradas, M., Martin, M., Tusell, L. & Genesca, A. Genetic activities in micronuclei: is the DNA entrapped in micronuclei lost for the cell? *Mutat Res* **705**, 60-67 (2010). https://doi.org:10.1016/j.mrrev.2010.03.004

17 Schenkel, L., Wang, X., Le, N., Burger, M. & Kroschewski, R. A dedicated cytoplasmic container collects extrachromosomal DNA away from the mammalian nucleus. *Molecular Biology of the Cell* **34**, ar105 (2023). https://doi.org:10.1091/mbc.E23-04-0118

18 Ly, P. *et al.* Chromosome segregation errors generate a diverse spectrum of simple and complex genomic rearrangements. *Nat Genet* **51**, 705-715 (2019). https://doi.org:10.1038/s41588-019-0360-8

19 Umbreit, N. T. *et al.* Mechanisms generating cancer genome complexity from a single cell division error. *Science* **368** (2020). https://doi.org:10.1126/science.aba0712

20 Zhang, C. Z. *et al.* Chromothripsis from DNA damage in micronuclei. *Nature* **522**, 179-184 (2015). https://doi.org:10.1038/nature14493

21 Agustinus, A. S. *et al.* Epigenetic dysregulation from chromosomal transit in micronuclei. *Nature* **619**, 176-183 (2023). https://doi.org:10.1038/s41586-023-06084-7

22 Papathanasiou, S. *et al.* Heritable transcriptional defects from aberrations of nuclear architecture. *Nature* **619**, 184-192 (2023). https://doi.org:10.1038/s41586-023-06157-7

23 Hatch, E. M., Fischer, A. H., Deerinck, T. J. & Hetzer, M. W. Catastrophic nuclear envelope collapse in cancer cell micronuclei. *Cell* **154**, 47-60 (2013). https://doi.org:10.1016/j.cell.2013.06.007

24 Von Hoff, D. D. *et al.* Hydroxyurea accelerates loss of extrachromosomally amplified genes from tumor cells. *Cancer Res* **51**, 6273-6279 (1991).

25 Von Hoff, D. D. *et al.* Elimination of extrachromosomally amplified MYC genes from human tumor cells reduces their tumorigenicity. *Proc Natl Acad Sci U S A* **89**, 8165-8169 (1992). https://doi.org:10.1073/pnas.89.17.8165

26 Shimizu, N., Itoh, N., Utiyama, H. & Wahl, G. M. Selective entrapment of extrachromosomally amplified DNA by nuclear budding and micronucleation during S phase. *J Cell Biol* **140**, 1307-1320 (1998). https://doi.org:10.1083/jcb.140.6.1307

27 Hung, K. L. *et al.* Coordinated inheritance of extrachromosomal DNAs in cancer cells. *Nature* **635**, 201-209 (2024). https://doi.org:10.1038/s41586-024-07861-8

28 Nichols, A. *et al.* Chromosomal tethering and mitotic transcription promote ecDNA nuclear inheritance. *Molecular Cell* **85**, 2839-2853.e2838 (2025). https://doi.org:https://doi.org/10.1016/j.molcel.2025.06.013

29 Tang, J. *et al.* Enhancing transcription–replication conflict targets ecDNA-positive cancers. *Nature* **635**, 210-218 (2024). https://doi.org:10.1038/s41586-024-07802-5

30 Jaworski, J. J. *et al.* ecDNA replication is disorganized and vulnerable to replication stress. *Nucleic Acids Res* **53** (2025). https://doi.org:10.1093/nar/gkaf711

31 Trivedi, P., Steele, C. D., Au, F. K. C., Alexandrov, L. B. & Cleveland, D. W. Mitotic tethering enables inheritance of shattered micronuclear chromosomes. *Nature* **618**, 1049-1056 (2023). https://doi.org:10.1038/s41586-023-06216-z

32 Lin, Y. F. *et al.* Mitotic clustering of pulverized chromosomes from micronuclei. *Nature* **618**, 1041-1048 (2023). https://doi.org:10.1038/s41586-023-05974-0

33 Giurgiu, M. *et al.* Reconstructing extrachromosomal DNA structural heterogeneity from long-read sequencing data using Decoil. *Genome Res* **34**, 1355-1364 (2024). https://doi.org:10.1101/gr.279123.124

34 Tanaka, T. & Shimizu, N. Induced detachment of acentric chromatin from mitotic chromosomes leads to their cytoplasmic localization at G(1) and the micronucleation by lamin reorganization at S phase. *J Cell Sci* **113 (Pt 4)**, 697-707 (2000). https://doi.org:10.1242/jcs.113.4.697

35 Pradella, D. *et al.* Engineered extrachromosomal oncogene amplifications promote tumorigenesis. *Nature* **637**, 955-964 (2025). https://doi.org:10.1038/s41586-024-08318-8

36 Ahmed, A., Isaksen, T. J. & Yamashita, T. Protocol for mouse adult neural stem cell isolation and culture. *STAR Protoc* **2**, 100522 (2021). https://doi.org:10.1016/j.xpro.2021.100522

37 MacArthur, I. C. *et al.* Prohibitin promotes de-differentiation and is a potential therapeutic target in neuroblastoma. *JCI Insight* **5** (2019). https://doi.org:10.1172/jci.insight.127130

38 Bahry, E. *et al.* RS-FISH: precise, interactive, fast, and scalable FISH spot detection. *Nat Methods* **19**, 1563-1567 (2022). https://doi.org:10.1038/s41592-022-01669-y

39 Von Hoff, D. D. *et al.* Elimination of extrachromosomally amplified MYC genes from human tumor cells reduces their tumorigenicity. *Proceedings of the National Academy of Sciences* **89**, 8165-8169 (1992). https://doi.org:doi:10.1073/pnas.89.17.8165

40 Li, H. Minimap2: pairwise alignment for nucleotide sequences. *Bioinformatics* **34**, 3094-3100 (2018). https://doi.org:10.1093/bioinformatics/bty191

41 Jones, M. J. K. *et al.* A high-resolution, nanopore-based artificial intelligence assay for DNA replication stress in human cancer cells. *Nat Commun* **16**, 7732 (2025). https://doi.org:10.1038/s41467-025-63168-w

42 Boeva, V. *et al.* Heterogeneity of neuroblastoma cell identity defined by transcriptional circuitries. *Nat Genet* **49**, 1408-1413 (2017). https://doi.org:10.1038/ng.3921

43 Winick-Ng, W. *et al.* Cell-type specialization is encoded by specific chromatin topologies. *Nature* **599**, 684-691 (2021). https://doi.org:10.1038/s41586-021-04081-2

44 Irastorza-Azcarate, I. *et al.* Extensive folding variability between homologous chromosomes in mammalian cells. *bioRxiv*, 2024.2005.2008.591087 (2024). https://doi.org:10.1101/2024.05.08.591087

45 Shafin, K. *et al.* Nanopore sequencing and the Shasta toolkit enable efficient de novo assembly of eleven human genomes. *Nat Biotechnol* **38**, 1044-1053 (2020). https://doi.org:10.1038/s41587-020-0503-6

46 Krueger, F., James, F., Ewels, P., Afyounian, E. & Schuster-Boeckler, B. TrimGalore v.0.6.10. *https://zenodo.org/records/7598955* (2021).

47 Li, H. Aligning sequence reads, clone sequences and assembly contigs with BWA-MEM. *arXiv:1303.3997 [q-bio.GN]* (2013).

48 Picard toolkit. *Broad Institute, GitHub repository* **https://broadinstitute.github.io/picard/** (2019).

49 Ramirez, F. *et al.* deepTools2: a next generation web server for deep-sequencing data analysis. *Nucleic Acids Res* **44**, W160-165 (2016). https://doi.org:10.1093/nar/gkw257

50 Beagrie, R. A. *et al.* Complex multi-enhancer contacts captured by genome architecture mapping. *Nature* **543**, 519-524 (2017). https://doi.org:10.1038/nature21411

51 Delignette-Muller, M. L. & Dutang, C. fitdistrplus: An R Package for Fitting Distributions. *Journal of Statistical Software* **64**, 1 - 34 (2015). https://doi.org:10.18637/jss.v064.i04

52 Talevich, E., Shain, A. H., Botton, T. & Bastian, B. C. CNVkit: Genome-Wide Copy Number Detection and Visualization from Targeted DNA Sequencing. *PLoS Comput Biol* **12**, e1004873 (2016). https://doi.org:10.1371/journal.pcbi.1004873

53 Pagès H, A. P., Gentleman R, DebRoy S. Biostrings: Efficient manipulation of biological strings version 2.66.0. *https://bioconductor.org/packages/Biostrings* (2022).

54 Seshan VE, O. A. DNAcopy: DNA copy number data analysis version 1.72.3. *https://bioconductor.org/packages/DNAcopy* (2023).
55 H, W. *ggplot2: Elegant Graphics for Data Analysis.*, (Springer-Verlag New York., 2016).
56 Signorell, A. DescTools: Tools for Descriptive Statistics. *https://CRAN.R-project.org/package=DescTools* (2024). https://doi.org:10.32614/CRAN.package.DescTools
57 Kharchenko, P. V., Tolstorukov, M. Y. & Park, P. J. Design and analysis of ChIP-seq experiments for DNA-binding proteins. *Nat Biotechnol* **26**, 1351-1359 (2008). https://doi.org:10.1038/nbt.1508
58 Landt, S. G. *et al.* ChIP-seq guidelines and practices of the ENCODE and modENCODE consortia. *Genome Res* **22**, 1813-1831 (2012). https://doi.org:10.1101/gr.136184.111
59 Dobin, A. *et al.* STAR: ultrafast universal RNA-seq aligner. *Bioinformatics* **29**, 15-21 (2013). https://doi.org:10.1093/bioinformatics/bts635
60 Anders, S., Pyl, P. T. & Huber, W. HTSeq--a Python framework to work with high-throughput sequencing data. *Bioinformatics* **31**, 166-169 (2015). https://doi.org:10.1093/bioinformatics/btu638
61 Love, M. I., Huber, W. & Anders, S. Moderated estimation of fold change and dispersion for RNA-seq data with DESeq2. *Genome Biol* **15**, 550 (2014). https://doi.org:10.1186/s13059-014-0550-8
62 Yu, G., Wang, L. G., Han, Y. & He, Q. Y. clusterProfiler: an R package for comparing biological themes among gene clusters. *OMICS* **16**, 284-287 (2012). https://doi.org:10.1089/omi.2011.0118
63 Yu, G., Wang, L. G., Yan, G. R. & He, Q. Y. DOSE: an R/Bioconductor package for disease ontology semantic and enrichment analysis. *Bioinformatics* **31**, 608-609 (2015). https://doi.org:10.1093/bioinformatics/btu684
64 Simon, T. *et al.* Long term outcome of high-risk neuroblastoma patients after immunotherapy with antibody ch14.18 or oral metronomic chemotherapy. *BMC Cancer* **11**, 21 (2011). https://doi.org:10.1186/1471-2407-11-21
65 Berthold, F. *et al.* Myeloablative megatherapy with autologous stem-cell rescue versus oral maintenance chemotherapy as consolidation treatment in patients with high-risk neuroblastoma: a randomised controlled trial. *Lancet Oncol* **6**, 649-658 (2005). https://doi.org:10.1016/S1470-2045(05)70291-6
66 Kaplan, E. L. & Meier, P. Nonparametric-Estimation from Incomplete Observations. *J Am Stat Assoc* **53**, 457-481 (1958). https://doi.org:Doi 10.2307/2281868
67 Savage, J. R. A comment on the quantitative relationship between micronuclei and chromosomal aberrations. *Mutat Res* **207**, 33-36 (1988). https://doi.org:10.1016/0165-7992(88)90008-5

1227

Main Figures

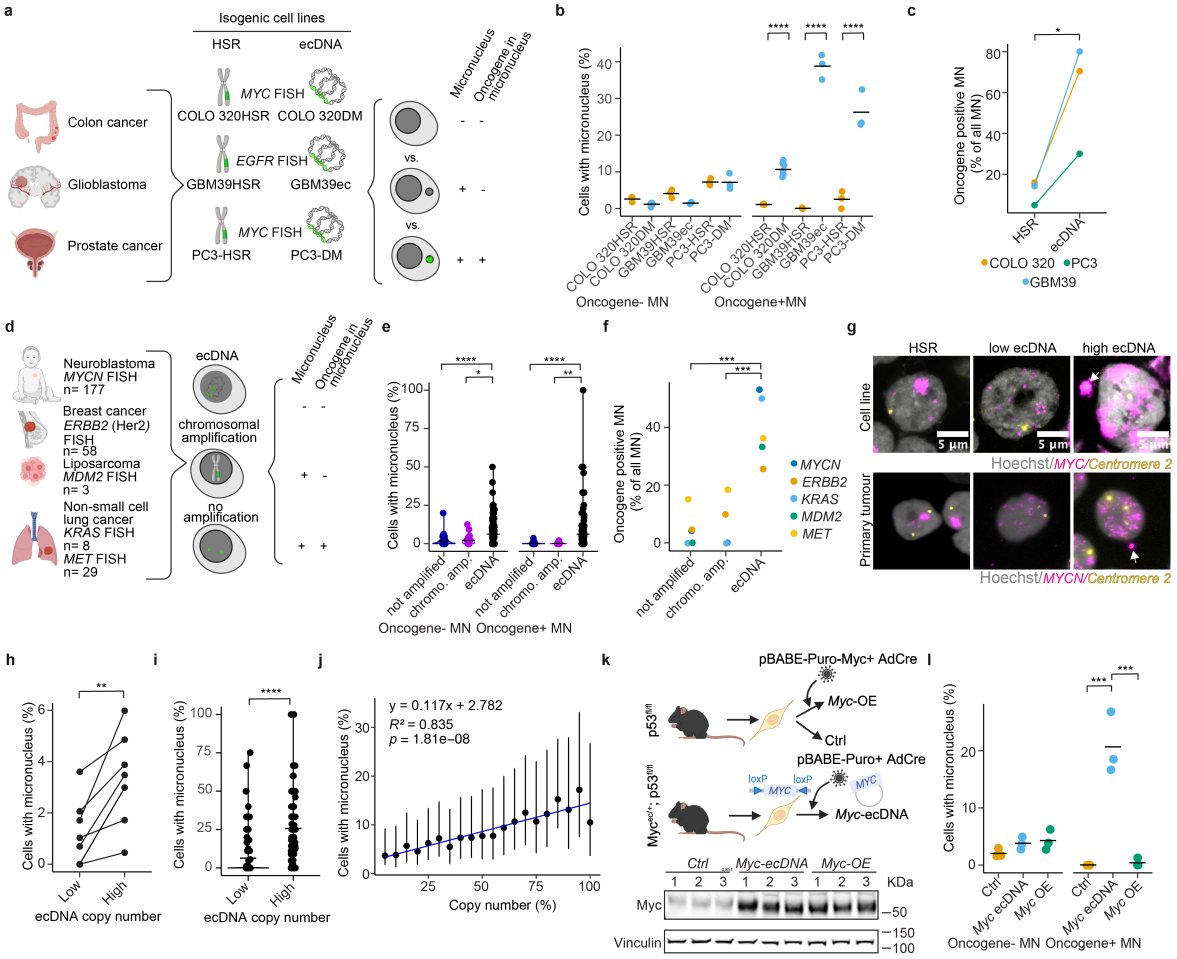

Fig 1. Cancer cells with ecDNA more frequently have micronuclei than cells with chromosomal amplifications.
a. Schematic of the experimental design to quantify micronuclei in near-isogenic cancer cell lines.
b. Fraction of cells with oncogene-negative and oncogene-positive micronuclei in 3 near-isogenic cell line pairs (n= 6 cell lines), as determined using oncogene-specific FISH. Each dot donates one experimental replicate (n = 2–5 experiments per cell line, n= 37-837 cells per replicate; Student's *t*-test).
c. Fraction of micronuclei containing the amplified oncogene in near-isogenic cell lines (n = 3 isogenic cell line pairs, n= 25-522 micronuclei per cell line). Each dot represents one cell line.
d. Schematic of the experimental design to quantify micronuclei in patient biopsies.
e. Fraction of cells with oncogene-negative and oncogene-positive micronuclei in primary tumours with ecDNA, chromosomal amplification or without amplification (n = 236 tumours; n= 5-574 cells per tumour sample; Kruskal-Wallis-test), as determined using oncogene-specific FISH. Each dot denotes one patient sample.
f. Fraction of micronuclei containing the amplified oncogene across patient cohorts stratified by oncogene (Student's *t*-test).
g. Exemplary micrographs of cell line and *MYCN*- amplified Neuroblastoma tumour sample with an HSR (cell line: COLO 320HSR), low ecDNA content or high ecDNA content (cell line: both COLO 320DM) and micronuclei (arrowheads) stained with Hoechst (grey), *MYCN*-specific FISH (magenta) and chromosome 2 centromeric FISH (yellow).
h-i. Fraction of micronucleated cells in the cells with low (bottom 30%, n= 5- 192 cells) and high (top 30%, n= 5- 192 cells) ecDNA content in cell lines (n = 7 cell lines, COLO 320DM, CHP-212, STA-NB10DM, Tr-14, UKF-NB6, Lan5, SMS-KAN (paired Student's *t*-test) h) and in primary tumours (n = 148, Kruskal-Wallis-test) (i);). Each dot corresponds to one cell line (h) or one patient sample (i).
j. Combined cell line and tumour cell fraction from (h) and (i) with micronuclei and their ecDNA copy number. For each dataset, overall ecDNA copy number as determined by FISH was partitioned into deciles, and micronucleation frequency was calculated within each bin (n = 148 tumours, n= 7 cell lines).
k. Experimental design to induce ecDNA in mouse aNSCs (top), and Myc immunoblot (bottom) in three independent *Myc* ecDNA-containing cells (*Myc*-ecDNA) and *Myc*-overexpressing (*Myc*-OE) cells compared to control cells (Ctrl) without ecDNA and not expressing Myc, respectively.
l. Fraction of cells with *Myc*-negative (oncogene-negative) and *Myc*-positive (oncogene-positive) micronuclei in *Myc*-ecDNA cells, *Myc*-OE or control aNSCs, as determined by *Myc*-specific FISH and Hoechst staining. Each dot denotes one independent experiment (n = 3; one-way ANOVA).

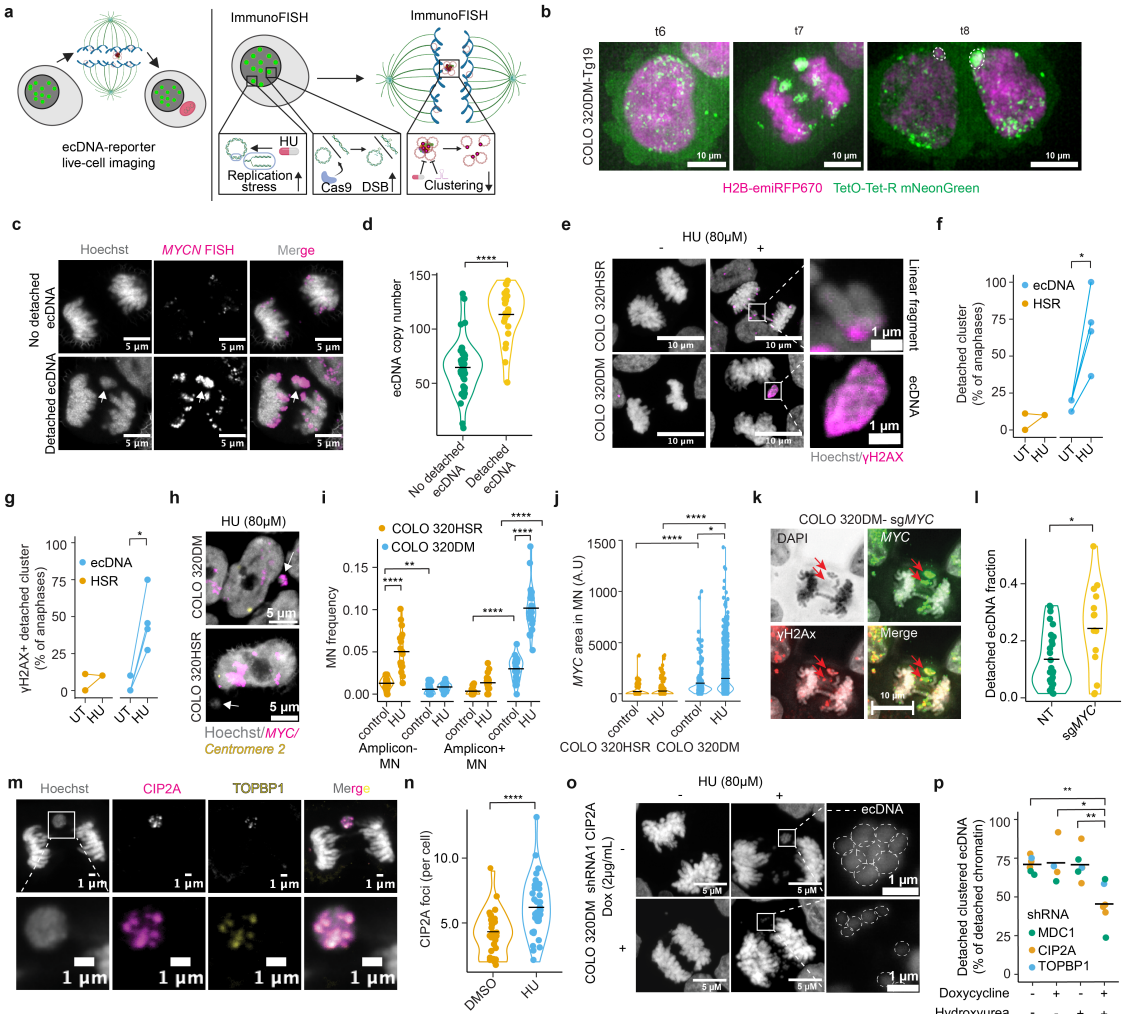

Fig 2. Replication stress induces MDC1-CIP2A-TOPBP1-associated clustered detachment and micronucleation.

a. Schematic of experimental design. Live-cell imaging of COLO 320DM-Tg19 cells with fluorescently tagged ecDNA was used to evaluate detachment and micronucleation of ecDNA. FISH combined with immunofluorescence (ImmunoFISH) in fixed interphase and anaphase cells was used to measure replication stress, DNA damage and MDC1-CIP2A-TOPBP1 on ecDNA clusters in mitosis following genetic and pharmacologic perturbations.

b. Exemplary photomicrographs taken during live cell imaging of a COLO 320DM-Tg19 cell engineered to visualize *MYC* ecDNA (TetO-TetR-mNeonGreen) during mitotic transition. Cell with ecDNA (green) within its primary nucleus (magenta) before mitosis (left), during anaphase (middle) and after mitosis (right). Dotted lines indicate micronuclei, which were confirmed to be outside the primary nucleus. Scale bar: 10μm.

c. Exemplary micrographs of fixed, untreated CHP212 cells that contain *MYCN* ecDNA during anaphase with (bottom) or without (top) detached ecDNA cluster, stained with Hoechst (grey) and *MYCN* DNA FISH (magenta).

d. Number of ecDNA copies per cell in CHP212 cells with detached ecDNA clusters during anaphase in untreated cells compared to those cells without such detached clusters. Each dot denotes one anaphase (n = 52; Student's *t*-test). Black line indicates average in all plots.

e. Exemplary photomicrographs of representative fixed COLO 320DM (contains *MYC* as ecDNA, bottom) and COLO 320HSR (contains *MYC* as HSR, top) cells in anaphase that were incubated in the presence or absence of HU (80μM) for 3 days and stained with Hoechst and for γH2AX. Scale bar: 5μm

f. Frequency of DNA clusters during anaphase as measured using Hoechst staining of fixed cells in cell lines with ecDNA (n= 4 independent cell lines) compared to cell lines with HSRs (n=2 independent cell lines) in the presence (HU) or absence (UT) of hydroxyurea (80 μM) (n=10-15 anaphases per cell line and treatment group). Each dot represents the average fraction of cells with a DNA cluster per cell line.

g. Frequency of detached chromatin clusters positively staining for γH2AX in cell lines containing ecDNA (n=4 independent cell lines) compared to cells with HSRs (n=2 independent cell lines) incubated in the presence or absence of hydroxyurea (80 μM, 24h) (n=10-15 anaphases per cell line and treatment group were assessed). Each dot represents the average per cell line.

h. Exemplary photomicrographs of representative fixed COLO 320DM containing *MYC* ecDNA and COLO 320SHR containing *MYC* HSR, stained with *MYC* FISH after 3d HU (80μM). White arrows indicate MN. Scale bar: 5μm

i. Fraction of COLO 320DM and COLO 320HSR cells with oncogene- versus oncogene^{+} MN based on oncogene-specific FISH in the presence or absence of HU (50 μM; n= 20-26 MN; Two- way ANOVA). Each dot represents one image.

j. Quantification of *MYC* FISH signal in micronuclei in the presence of HU (3d, 50μM) in COLO 320DM compared to COLO 320HSR cells (n = 100–923 MN; Wilcox test). Each dot denotes one MN.

k. Exemplary photomicrographs of COLO 320DM cells after CRISPR-Cas9 mediated cutting of *MYC,* which is present on ecDNA in these cells, and stained with DAPI (grey), *MYC* FISH (green), γH2AX immunofluorescence (red) as well as a merged image.

l. Fraction of detached ecDNA in anaphase, measured using *MYC* FISH in COLO 320DM cells 24hrs after nucleofection of Cas9 and a guide RNA targeting *MYC (sgMYC,* n=15*)* compared to cells expressing a scrambled sgRNA control (sgNT, n=27) (Student's t-test).

m. Exemplary photomicrographs of a COLO 320DM cell with ecDNA in anaphase (top) as well as an enlarged view of DNA cluster (bottom) stained with Hoechst (grey) and immunofluorescence for TOPBP1 (yellow) or CIP2A (magenta).

n. Quantification of immunofluorescent CIP2A foci in COLO 320DM anaphase cells after incubation in the presence of HU (100 µM) for 24hrs compared to untreated cells (n = 31–33 anaphases; Student's t-test). Each dot denotes one anaphase.
o. Exemplary photomicrographs of COLO 320DM cells transduced to inducibly express an shRNA targeting CIP2A in the presence (bottom) or absence (top) of doxycycline (2 µg/ml, 2 days) and in the presence (right) or absence (left) of HU (80 µM, 24 h) in anaphase. Scale bar: 5 µm. Dotted circles represent outlines of small chromatin bodies representing ecDNA.
p. Fraction of clustered chromatin as measured using Hoechst staining in cells harbouring ecDNA and inducibly expressing shRNAs targeting MDC1 (two independent sgRNAs, green), TOPBP1 (1 shRNA, blue), or CIP2A (3 independent shRNAs, orange) in the presence or absence of either doxycycline (2µg/ml, 2 days) and/or HU (80µM, 24h) in COLO 320DM cells (n = 10–12 anaphases per condition; one-way ANOVA). Each dot denotes the mean per anaphase. Line indicates the mean.

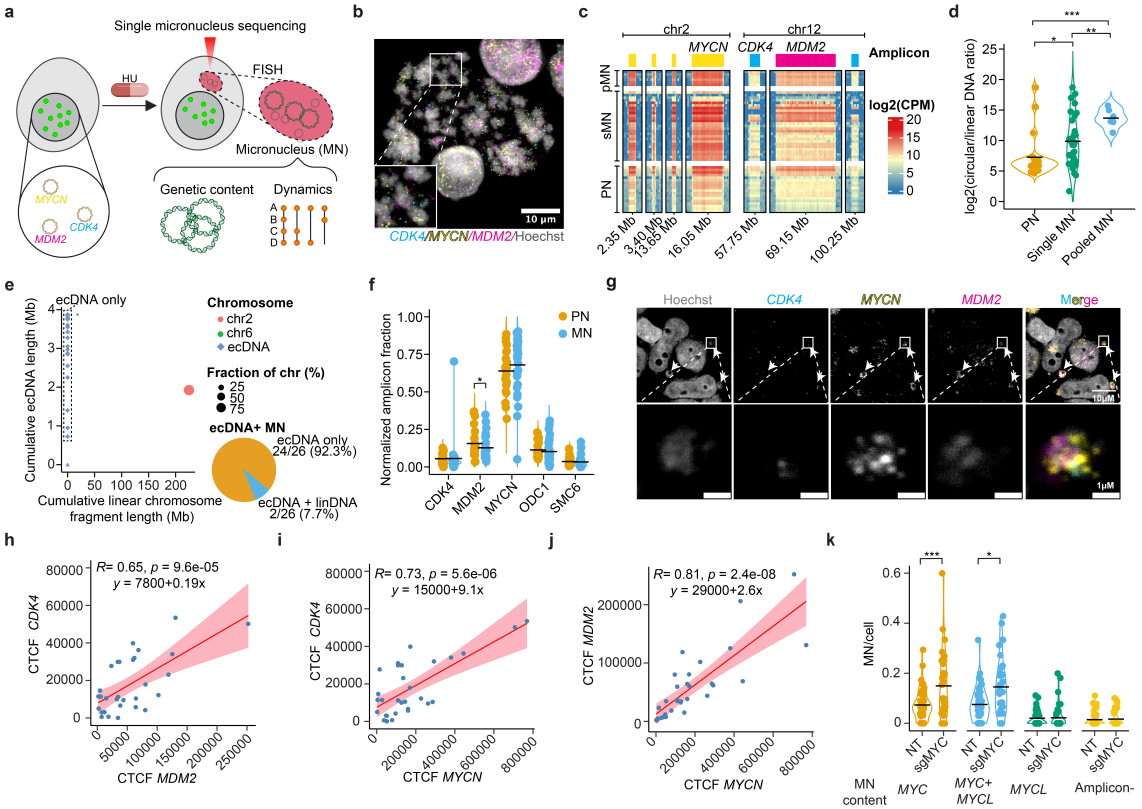

Fig 3. Collective entrapment of distinct ecDNAs in the same micronuclei.

a. Experimental design. Laser microdissection (red triangle) was used to isolate micronuclei or primary nuclei, which was followed by sequencing. FISH was used to validate findings.

b. Exemplary photomicrograph of a metaphase spread of a TR-14 cell stained with Hoechst (grey) and FISH for oncogenes (*CDK4,* blue; *MYCN,* yellow; *MDM2,* red*)* present on distinct ecDNA species.

c. Laser microdissection directed sequencing of primary nuclei (PN) and micronuclei (MN) after incubation of TR-14 cells in the presence of HU (80 µM). Counts per million (CPM), normalized and log2 transformed read coverage (25kb bins) across ecDNA (*CDK4,* blue; *MYCN,* yellow; *MDM2,* red*)* and their flanking regions (100 kb; primary nucleus, PN, n = 18; single micronucleus, sMN, n = 27; pooled micronuclei, pMN, n = 6).

d. Log2-transformed mean coverage ratio of circular reads over the winsorized mean of all linear reads in PN, sMN and pMN (Welch's t-test).

e. Cumulative ecDNA and linear chromosome length of enriched fragments in single micronuclei. Size of linear chromosomal fragments (dots) denotes fraction of the incorporated whole chromosome or chromosomal fragment. Bottom right: fraction of ecDNA positive MN containing either only ecDNA or ecDNA and linear chromatin.

f. Amplicon-size normalized fraction of circular reads mapping to specific ecDNA species in primary nuclei (n=18) and micronuclei (n=27) (Permutation test, 10000 permutations, one-sided).

g. Exemplary photomicrograph of a micronucleus in the TR-14 cell line harbouring multiple ecDNA, stained for *CDK4, MYCN* and *MDM2* using FISH.

h-j. Correlation between normalised corrected total cell fluorescence (CTCF) from FISH in micronuclei for *CDK4* and *MDM2* (h), *CDK4* and *MYCN* (i), *MDM2* and *MYCN* (j).

k. Frequency of micronuclei per cell in DMS273 cells 24h after expression of Cas9 and sgRNA targeting *MYC* (sgMYC) or a scrambled sgRNA (NT) and stained with DAPI and oncogene-specific FISH for *MYC* or *MYCL* to classify MN according to their ecDNA content (n= 38-48, Wilcox test). Each dot represents one image.

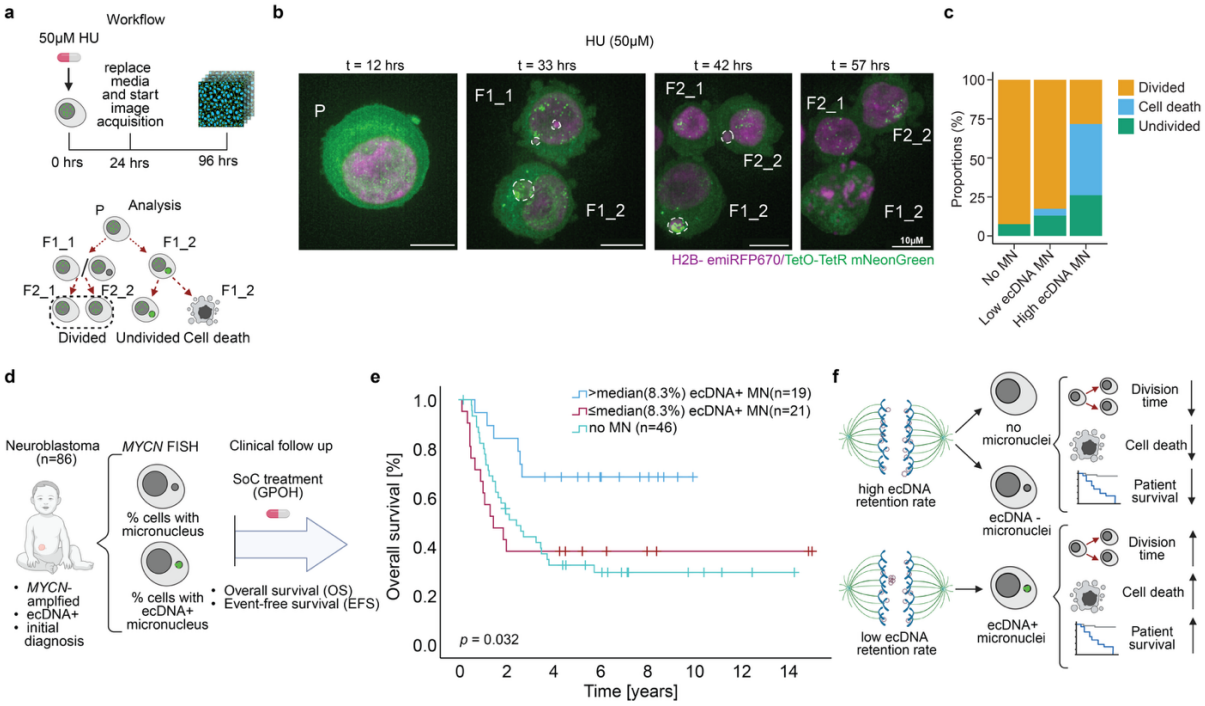

Fig. 4: The presence of ecDNA in micronuclei is associated with reduced cancer cell fitness and improved patient outcome.
a. Experimental design for live-cell imaging and analysis. Cells were tracked for two generations, from the parental cell (P), to generation F1, daughter cells (F1_1 and F1_2) to generation F2, granddaughter cells (F2_1 and F2_2).
b. Representative frames from time-lapse imaging of a COLO 320DM-Tg19 parental cell (P, left) undergoing cell division twice (F1 and F2 generations) in the presence of HU (50µM), in which *MYC* ecDNA (green) and chromatin (magenta) are fluorescently labelled. Micronuclei are marked with dotted lines and were confirmed in 3D reconstructions to be outside the nucleus. Cell with ecDNA-containing MN (F1_2) exhibits nuclear blebbing at t=57h, indicative of cell death. Scale bar: 10 µm.
c. Quantification of COLO 320DM-Tg19 cell fates as determined using live cell imaging in the presence of HU (50µM) for cells without micronuclei (No MN), with MN containing low ecDNA content (below median; low ecDNA MN), or with MN containing high ecDNA content (above median; high ecDNA MN). Cell fates include cell division, cell death, or remaining undivided (n = 143 individual cells at the end of the 72h imaging period).
d. Schematic overview of the analysis of 86 *MYCN* ecDNA-positive neuroblastoma biopsies, in which the presence of micronuclei and their content was determined using *MYCN* FISH and DAPI staining (registered in the trials NB97, n = 2; NB04, n = 67; NB2016, n = 17). Median follow-up, 6.8 years (range 0.14–15.9) for 36 survivors.
e. Kaplan–Meier survival curves for patients with more than 8.3% cells (median) in their biopsy with ecDNA-containing micronuclei (ecDNA$^+$ MN), patients with less than 8.3% ecDNA$^+$ MN, or those patients without MN (no MN; log-rank test).
f. Summary schematic of the main findings.